

doi:10.14379/iodp.proc.359.101.2017

Expedition 359 summary¹



C. Betzler, G.P. Eberli, C.A. Alvarez Zarikian, M. Alonso-García, O.M. Bialik, C.L. Blättler, J.A. Guo, S. Haffen, S. Horozal, M. Inoue, L. Jovane, D. Kroon, L. Lanci, J.C. Laya, A. Ling Hui Mee, T. Lüdmann, M. Nakakuni, B.N. Nath, K. Niino, L.M. Petruny, S.D. Pratiwi, J.J.G. Reijmer, J. Reolid, A.L. Slagle, C.R. Sloss, X. Su, P.K. Swart, J.D. Wright, Z. Yao, and J.R. Young²

Keywords: International Ocean Discovery Program, IODP, *JOIDES Resolution*, Expedition 359, Site U1465, Site U1466, Site U1467, Site U1468, Site U1469, Site U1470, Site U1471, Site U1472, Maldives, Kardiva Channel, Goidhoo atoll, Indian Ocean paleoceanography, Oligocene, Miocene, Pliocene, Pleistocene, carbonate platform, carbonate platform drowning, celestine, dolomite, drift deposits, large benthic foraminifers, monsoon, sea level, sequence stratigraphy

Abstract

International Ocean Discovery Program Expedition 359 was designed to address changes in sea level and currents, along with monsoon evolution in the Indian Ocean. The Maldives archipelago holds a unique and mostly unread Indian Ocean archive of the evolving Cenozoic icehouse world. Cores from eight drill sites in the Inner Sea of the Maldives provide the tropical marine record that is key for better understanding the effects of this global evolution in the Indo-Pacific realm. In addition, the bank geometries of the carbonate archipelago provide a physical record of changing sea level and ocean currents. The bank growth occurs in pulses of aggradation and progradation that are controlled by sea level fluctuations during the early and middle Miocene, including the mid-Miocene Climate Optimum. A dramatic shift in development of the carbonate edifice from a sea level–controlled to a predominantly current-controlled system appears to be directly linked to the evolving Indian monsoon. This phase led to a twofold configuration of bank development: bank growth continued in some parts of the edifice, whereas in other places, banks drowned. Drowning steps seem to coincide with onset and intensification of the monsoon-related current system and subsequent deposition of contourite fans and large-scale sediment drifts. As such, the drift deposits will provide a continuous record of Indian monsoon development in the region of the Maldives.

A major focus of Expedition 359 was to date precisely the onset of the current system. This goal was successfully completed during the expedition. The second important outcome of Expedition 359 was groundtruthing the hypothesis that the dramatic, pronounced change in style of the carbonate platform sequence stacking was caused by a combination of relative sea level fluctuations and ocean

current system changes. These questions are directly addressed by the shipboard scientific data.

In addition, Expedition 359 cores will provide a complete Neogene $\delta^{13}\text{C}$ record of the platform and platform margin sediments and a comparison with pelagic records over the same time period. This comparison will allow assessment of the extent to which platform carbonates record changes in the global carbon cycle and whether changes in the carbon isotopic composition of organic and inorganic components covary and the implications this has on the deep-time record. This determination is important because such records are the only type that exists in deep time.

Introduction

Changes in oceanic circulation and sea level, along with onset and fluctuations of the Indian monsoon, characterize the Neogene. Located in the Indian Ocean, the Maldives carbonate edifice bears the tropical marine record of these changes. The archipelago is characterized by a double row of atolls encompassing a basin, the Maldives Inner Sea, connected to the open ocean through passages. The Maldives Inner Sea has served as a depositional center of current-controlled deposits (i.e., drifts) since the partial drowning of parts of the carbonate edifice during the middle Miocene. This sedimentary system of drowned platform parts and drifts was the target of International Ocean Discovery Program (IODP) Expedition 359, which aimed to reconstruct its paleoceanographic evolution over the past 26 My. The approach of Expedition 359 was to reconstruct this evolution from the combined physical record provided by the seismic data, the lithologic record in the neritic and hemipelagic deposits, and the chemical proxies within the sedimentary column. This reconstruction was achieved by drilling eight sites

¹ Betzler, C., Eberli, G.P., Alvarez Zarikian, C.A., Alonso-García, M., Bialik, O.M., Blättler, C.L., Guo, J.A., Haffen, S., Horozal, S., Inoue, M., Jovane, L., Kroon, D., Lanci, L., Laya, J.C., Ling Hui Mee, A., Lüdmann, T., Nakakuni, M., Nath, B.N., Niino, K., Petruny, L.M., Pratiwi, S.D., Reijmer, J.J.G., Reolid, J., Slagle, A.L., Sloss, C.R., Su, X., Swart, P.K., Wright, J.D., Yao, Z., and Young, J.R., 2017. Expedition 359 summary. In Betzler, C., Eberli, G.P., Alvarez Zarikian, C.A., and the Expedition 359 Scientists, *Maldives Monsoon and Sea Level*. Proceedings of the International Ocean Discovery Program, 359: College Station, TX (International Ocean Discovery Program). <http://dx.doi.org/10.14379/iodp.proc.359.101.2017>

² Expedition 359 Scientists' addresses.

MS 359-101: Published 4 May 2017

This work is distributed under the [Creative Commons Attribution 4.0 International](https://creativecommons.org/licenses/by/4.0/) (CC BY 4.0) license. 

Contents

- 1 Abstract
- 1 Introduction
- 4 Background
- 7 Site summaries
- 28 Preliminary scientific assessment
- 30 References

Table T1. Expedition 359 hole summary. mbsl = meters below sea level. [Download table in .csv format.](#)

Hole	Latitude	Longitude	Water depth (mbsl)	Cores (N)	Core recovered (m)	Recovery (%)	Drilled interval (m)	Total penetration (m)	Time on hole (h)	Time on site (days)	Comments
359-											
U1465A	4°55.9873'N	073°0.6786'E	515.01	11	76.6	70		76.6	21.84		Two water cores
U1465B	4°55.9862'N	073°0.6897'E	512.64	22	155.4	6	65.9	221.3	20.40		Offset 20 m east of Hole U1465A
U1465C	4°55.9865'N	073°0.7002'E	510.12	25	178.2	14	55.0	233.2	33.36		Offset 20 m east of Hole U1465B
Site U1465 totals:				58	410.2		120.9	531.1	75.60	3.15	
U1466A	4°55.9888'N	073°1.6785'E	518.09	50	326.2	75		326.2	55.68		
U1466B	4°55.9883'N	073°1.6893'E	517.14	56	495.7	18	314.0	809.7	103.44		
Site U1466 totals:				106	821.9		314.0	1135.9	159.12	6.63	
U1467A	4°51.0139'N	073°17.0200'E	487.49	4	32.0	98		32.0	12.72		
U1467B	4°51.0255'N	073°17.0204'E	487.49	77	617.2	91		617.2	74.16		Offset 20 m north of Hole U1467A
U1467C	4°51.0362'N	073°17.0197'E	487.28	35	332.1	80	381.9	714.0	61.20		Offset 20 m north of Hole U1467B
U1467D	4°51.0475'N	073°17.0201'E	487.23	21	199.5	102	1.5	201.0	13.20		Offset 20 m north of Hole U1467C
U1467E	4°51.0137'N	073°17.0312'E	487.42	0		0	714.0	714.0	59.04		Offset 20 m east of Hole U1467A
Site U1467 totals:				137	1180.8		1097.4	2278.2	220.32	9.18	
U1468A	4°55.9832'N	073°4.2780'E	521.50	110	873.7	53	1.0	874.7	93.84		
U1468B	4°55.9823'N	073°4.2888'E	521.45	0		0	874.7	874.7	59.52		
Site U1468 totals:				110	873.7		875.7	1749.4	153.36	6.39	
U1469A	4°54.4143'N	073°0.4910'E	426.93	17	161.1	3		161.1	20.64		
U1469B	4°54.4166'N	073°0.4694'E	426.91	3	29.4	2	122.0	151.4	12.72		
Site U1469 totals:				20	190.5		122.0	312.5	33.36	1.39	
U1470A	4°45.9828'N	072°59.0324'E	399.70	24	190.0	74		190.0	17.52		
U1470B	4°45.9818'N	072°59.0210'E	399.72	18	174.8	4	168.9	343.7	46.80		
Site U1470 totals:				42	364.8		168.9	533.7	64.32	2.68	
U1471A	4°45.9825'N	073°08.1358'E	419.40	82	685.1	53		685.1	66.72		
U1471B	4°45.9825'N	073°08.1263'E	420.29	1	6.7	99		6.7	18.24		
U1471C	4°45.9831'N	073°08.1147'E	419.19	19	178.8	95		178.8	15.36		
U1471D	4°45.9828'N	073°08.1035'E	419.19	6	57.0	100	1.0	58.0	9.84		
U1471E	4°45.9829'N	073°08.0929'E	419.19	43	407.4	42	596.3	1003.7	111.60		
Site U1471 totals:				151	1335.0		597.3	1932.3	221.73	9.24	
U1472A	4°46.2653'N	073°04.0111'E	379.34	34	251.9	93	0	251.9	28.80		
Site U1472 totals:				34	251.9		0	251.9	28.80	1.20	
Expedition 359 totals:				658	5428.8		3296.2	8725.0	956.64	39.86	

aligned into two transects covering shallow to deep-water deposits. Sites U1465, U1466, U1468, U1469, and U1470 were drilled to recover a sedimentary sequence encompassing a carbonate platform to drift succession (Oligocene to Pleistocene) (Table T1; Figures F1, F2, F3). Sites U1467, U1471, and U1472 recovered a Miocene to Pleistocene carbonate drift succession. The expedition built on a se-

ries of seismic data sets that image the different steps of carbonate platform evolution (R/V *Meteor* Cruise M74/4 NEOMA and R/V *Sonne* Cruise SO236 MALSTROM) and previously drilled Ocean Drilling Program (ODP) Site 716 (Leg 115) (Backman, Duncan, et al., 1988).

Figure F1. Operations and core recovery, Expedition 359. Eight sites (U1465–U1472) were drilled using the APC, XCB, and RCB systems. Five sites were logged. Percentages at bottom of holes are core recovery (Table T1). See **Operations** in the Site U1471 chapter (Betzler et al., 2017) for more information on MDHDS testing. mbsl = meters below sea level, NA = not applicable.

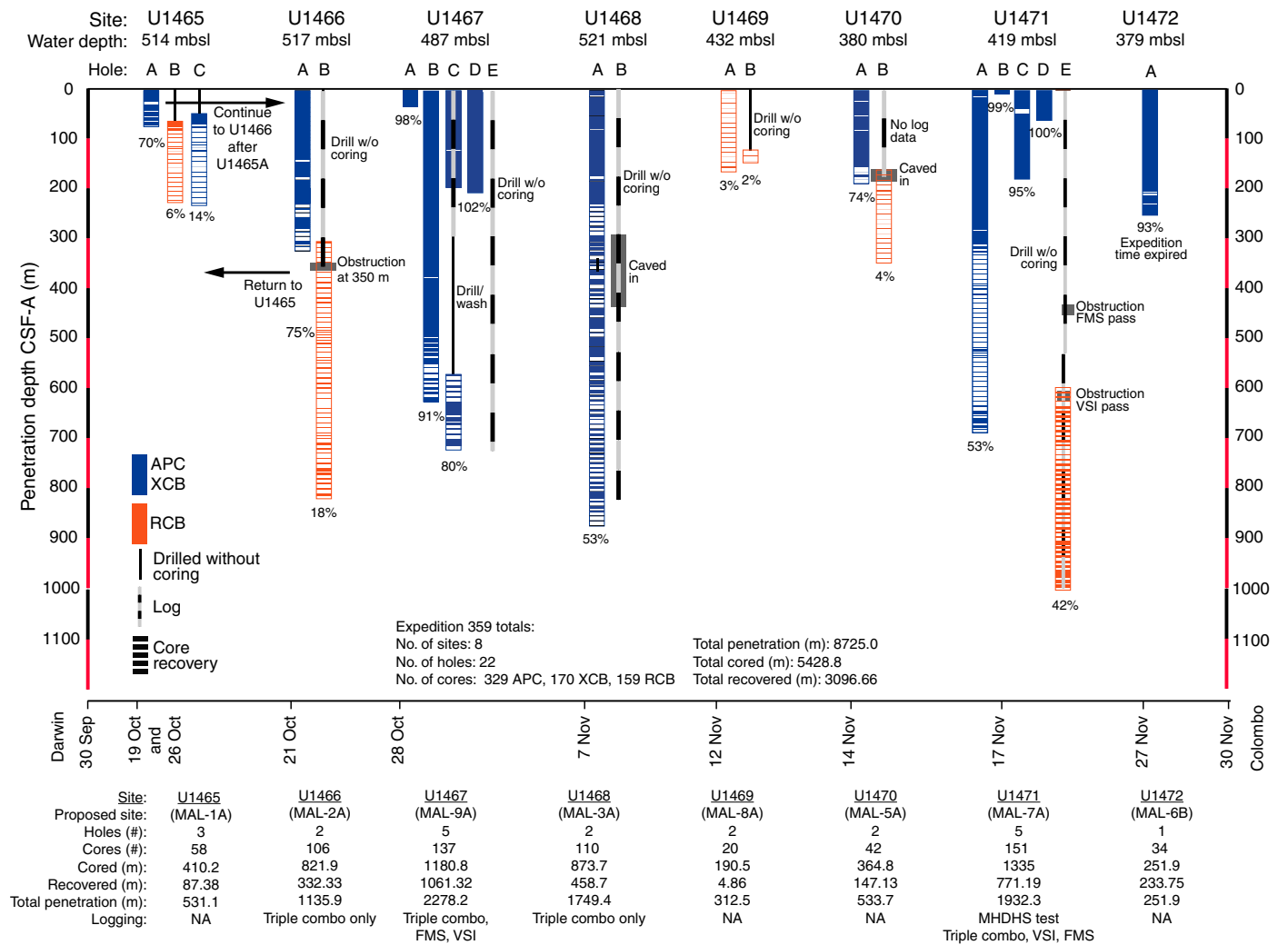


Figure F2. Lithostratigraphy and correlation of Expedition 359 northern transect sites with sequence boundaries. HSGR = variations of gamma ray intensity from downhole logs, NGR = variations of gamma ray intensity measured on the cores. Arag = aragonite, Dol = dolomite. This figure is available in an **oversized format**.

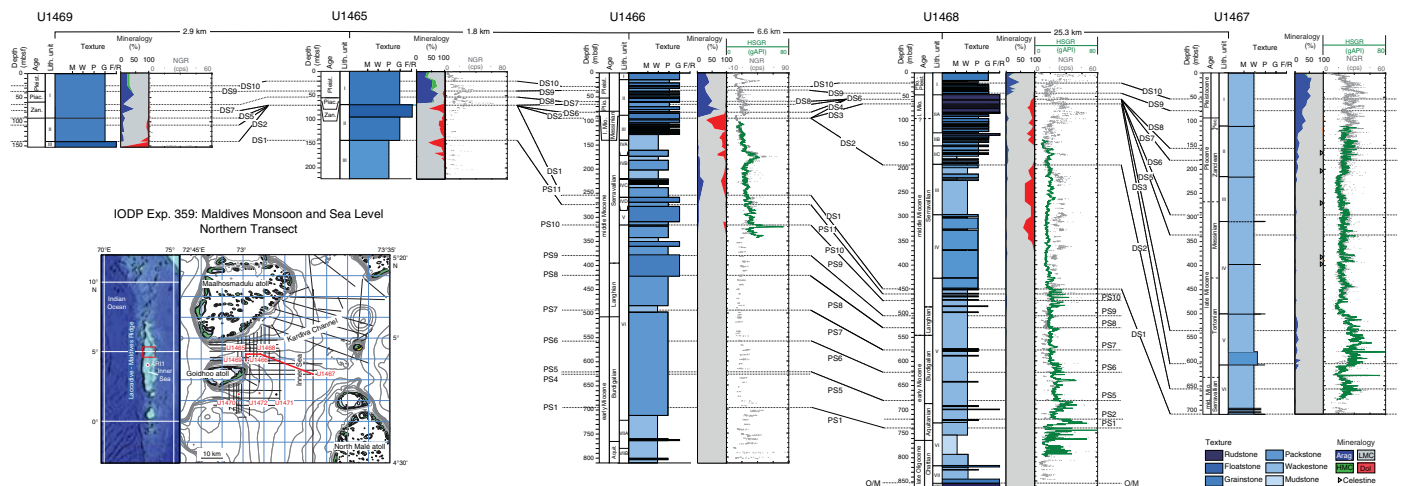
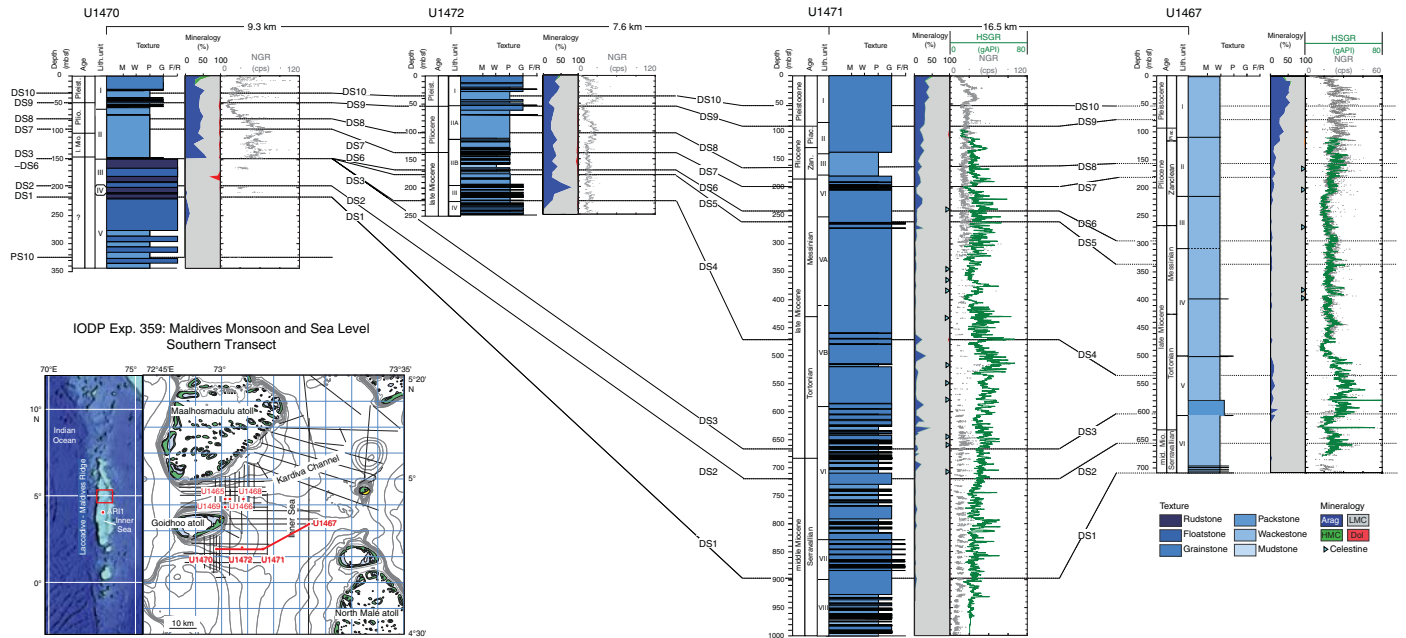


Figure F3. Lithostratigraphy and correlation of Expedition 359 southern transect sites with sequence boundaries. This figure is available in an [oversized format](#).



Background

Geological setting of the Maldives

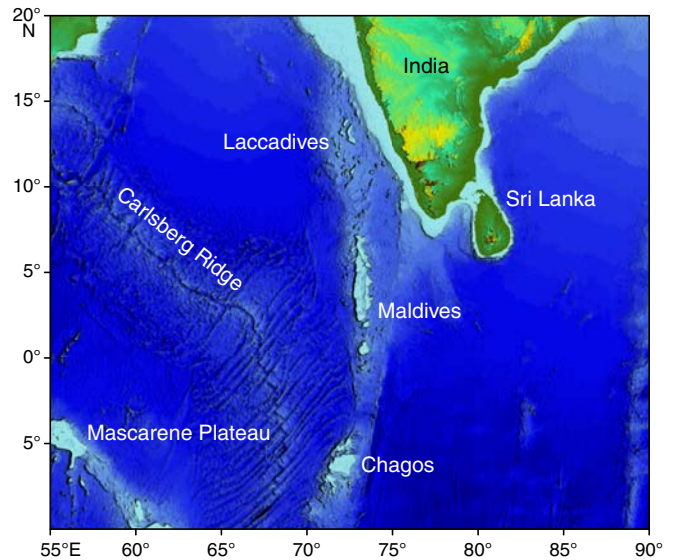
The Maldives archipelago in the central equatorial Indian Ocean is an isolated tropical carbonate platform edifice constituting the central and largest part of the Chagos-Laccadive Ridge, located southwest of India (Figure F4). A north-south-oriented double row of atolls encloses the Inner Sea of the Maldives (Figure F5). Intertoll channels that deepen toward the Indian Ocean separate the atolls from each other. The Inner Sea is a basin with water as deep as 550 m. The Maldives carbonate succession accumulated since the Eocene, away from any terrigenous input (Aubert and Droxler, 1992; Purdy and Bertram, 1993).

The modern archipelago comprises about 1200 smaller atolls that lie near or slightly above the sea surface. Discontinuous marginal rims formed by such small atolls surround lagoons with water depths to 50–60 m. These rims are interrupted by deep passages, allowing strong currents within the atoll lagoons to rework and re-deposit sediment and influence the growth of patch reefs (Ciarapica and Passeri, 1993; Betzler et al., 2015). Modern marginal reefs are composed of robust-branching corals and coralline algae, whereas the lagoonal reefs show domal corals and detrital sand and rubble facies (Gischler et al., 2008). Muddy sediments are present only in atoll areas that are protected by large marginal reefs (Ciarapica and Passeri, 1993; Gischler, 2006; Betzler et al., 2015).

The oceanward margins of the Maldives archipelago are generally steeply inclined, with dips of 20°–30° to 2000 m water depth. On the Inner Sea side, terraced atoll slopes have the same dip angles but reach water depths of only 150 m, where the gradient rapidly declines (Fürstenuau et al., 2010). The Inner Sea is characterized by periplatform ooze deposition that locally accumulates into sediment drift bodies (Droxler et al., 1990; Malone et al., 1990; Betzler et al., 2009, 2013a, 2013b; Paul et al., 2012; Lüdmann et al., 2013).

The climate and oceanographic settings of the Maldives are dictated by the seasonally reversing Indian monsoon system (Tomczak

Figure F4. Location map of the Maldives in the central equatorial Indian Ocean. The Maldives carbonate platform consists of 22 atolls on the Laccadive–Maldives Ridge, a volcanic ridge that formed when the Indian plate moved over the Réunion hotspot.



and Godfrey, 2003). Southwestern winds prevail during Northern Hemisphere summer (April–November), and northeastern winds prevail during winter (December–March). These winds generate ocean currents that are directed westward in the winter and eastward in the summer. Interseasonally, a band of Indian Ocean equatorial westerlies are established, enforcing strong eastward-flowing surface currents with velocities up to 1.3 m/s. Currents reach water depths of 200 m and more with only slightly reduced velocities (Tomczak and Godfrey, 2003). Within the modern atolls’ passages, currents can exhibit velocities up to 2 m/s at the surface (Preu and

Figure F5. Location map of Expedition 359 sites in the Inner Sea of the Maldives with line plan of site survey seismic lines for ARI 1, an existing industrial well that served for preexpedition seismic stratigraphic interpretation.

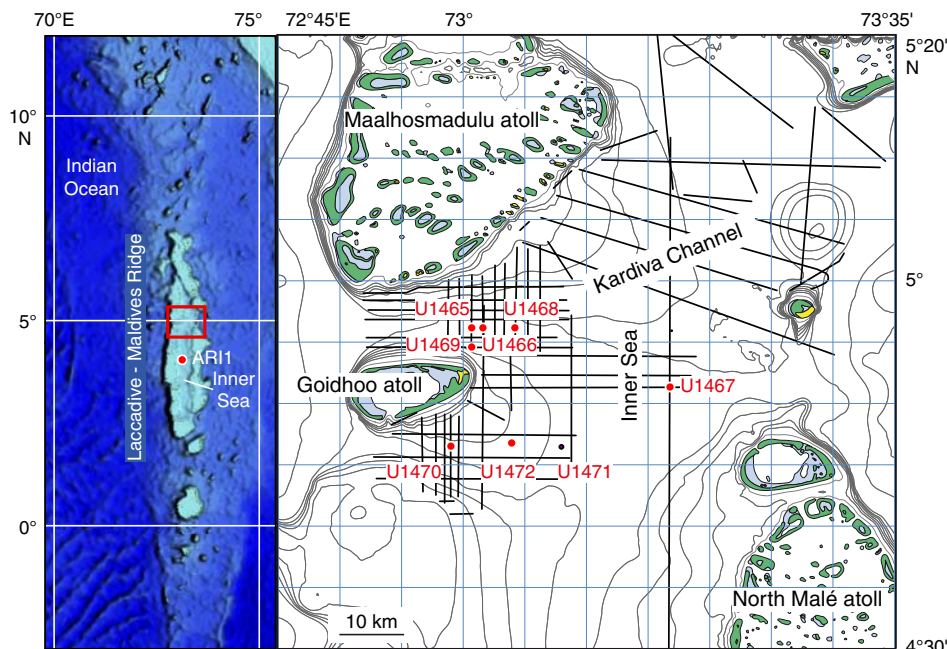
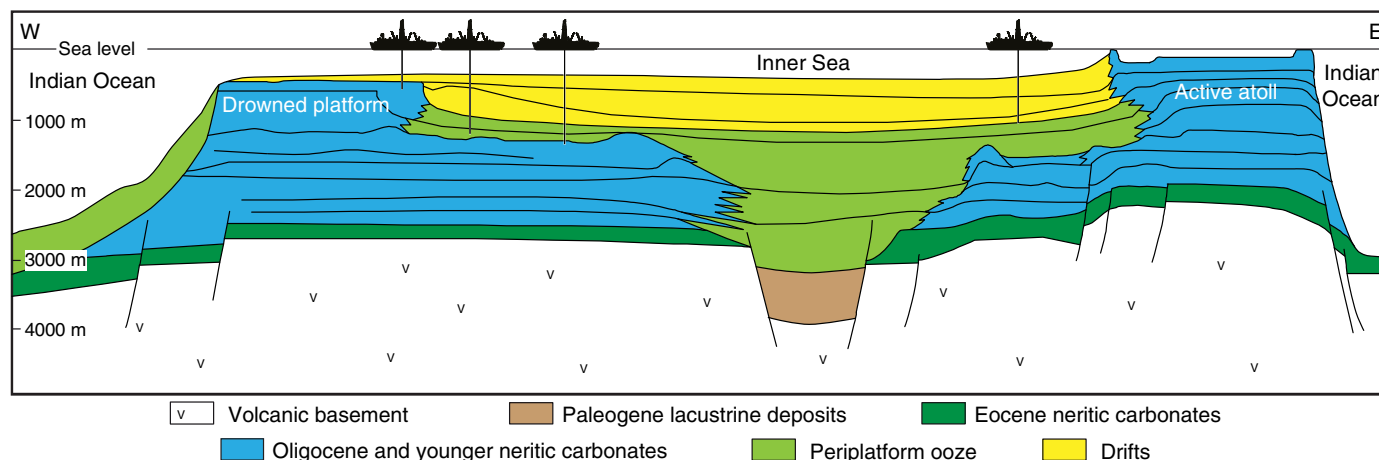


Figure F6. Sketch of the Maldives carbonate platform stratigraphy (after Betzler et al., 2013a). The volcanic basement is overlain by Eocene and Oligocene neritic carbonates. During the Oligocene, the platform areas shrank and two north-south-trending carbonate banks developed. During the Miocene, shallow-water carbonate banks partly drowned, whereas other platform areas grew further on. Contemporaneously, the carbonate platform was affected by an intensification of currents, as registered by the onset of widespread drift sedimentation in the Inner Sea of the Maldives. The research strategy for Expedition 359 was to drill two transects of sites from the inner part of the drowned platforms toward the Inner Sea, coring the platforms and the drifts.



Engelbrecht, 1991), accounting for winnowing in the passages and lagoons, where hard bottoms form (Ciarapica and Passeri, 1993; Gischler, 2006; Betzler et al., 2015).

The Maldives formed on a lower Paleogene (60–50 Ma) volcanic basement (Duncan and Hargraves, 1990) (Figure F6). The long-term subsidence rate of the Maldives is roughly 0.03–0.04 mm/y based on deep core data from Well ARI-1 (Aubert and Droxler, 1996; Belopolsky and Droxler, 2004a). In contrast, sedimentological data from the Rasdhoo atoll indicate a much faster subsidence rate since the last interglacial, with a maximum subsidence rate of 0.15 mm/y during the past 135,000 y (Gischler et al., 2008).

Lower to middle Miocene

The Maldives comprises an approximately 3 km thick shallow-water carbonate succession (Belopolsky and Droxler, 2004a) (Figure F6). Carbonate production was established during the early Eocene when flat-topped carbonate banks began to form on topographic highs created by the volcanic basement during the Eocene to early Oligocene. During the late Oligocene, bank margins typically had elevated rims that separated bank-interior areas from the open ocean. During the early Miocene, carbonate production became restricted to narrow bands at the respective most oceanward areas, forming the double row of platforms. During the Miocene, platform margins prograded toward the Inner Sea, as recognized in different

versions of seismic reflection data, irrespective of seismic resolution (Purdy and Bertram, 1993; Aubert and Droxler, 1996; Belopolsky and Droxler, 2004a; Betzler et al., 2009, 2013a).

Eleven seismic sequences are recognized in the lower and middle Miocene platform strata of the Maldives (Betzler et al., 2013a) (Figures F7, F8; see TRANSECTS in **Supplementary material**). These sequences are interpreted to have formed in response to sea level–driven accommodation space variations (Betzler et al., 2013a). Platform sequences (PS) PS1–PS6 show development from a shallow ramp to a steep-flanked, reef-rimmed carbonate platform. Bank-edge reefs protect the lagoon where back-reef aprons occur. At the PS6–PS7 transition, a switch from dominantly aggrading to dominantly prograding bank margins occurs. PS7–PS10 are com-

posed of deposits formed in response to forced regression and are overlain by deposits formed during reflooding of the bank margins.

Middle Miocene to Pleistocene

The upper middle Miocene is characterized by the appearance of large-scale lobate clinoform bodies, attesting to the onset of current-controlled deposition in the Inner Sea (Figures F7, F8) (Betzler et al., 2013a; Lüdmann et al., 2013). These bodies are attached to passages where some platforms drowned while remaining banks and atolls grew elsewhere (Betzler et al., 2009, 2013a). Lobes are fed by easterly currents and reworked by a current system flowing obliquely or normally to this main stream (Betzler et al., 2013a). This current pattern filled the Inner Sea from west to east (Lüd-

Figure F7. Expedition 359 northern transect with location of sites placed on the western part of seismic Line NEOMA-P65 (vertical exaggeration = 6x) running west–east through northern Kardiva Channel with sequence stratigraphic interpretation (Betzler et al., 2013a; Lüdmann et al., 2013) and age assignments.

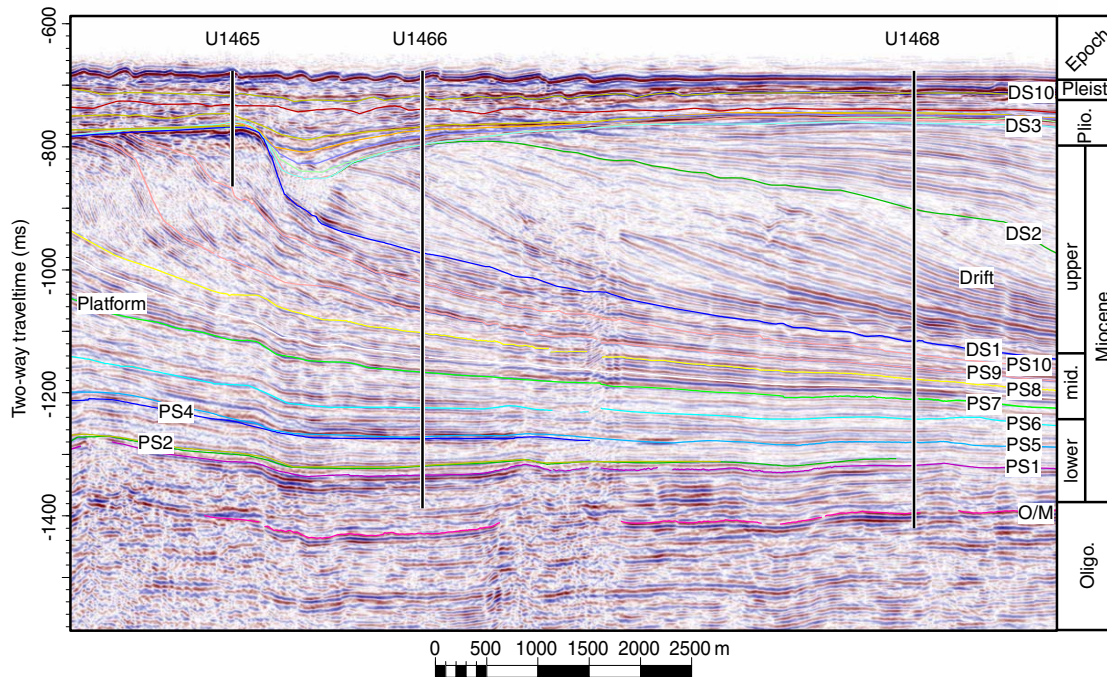
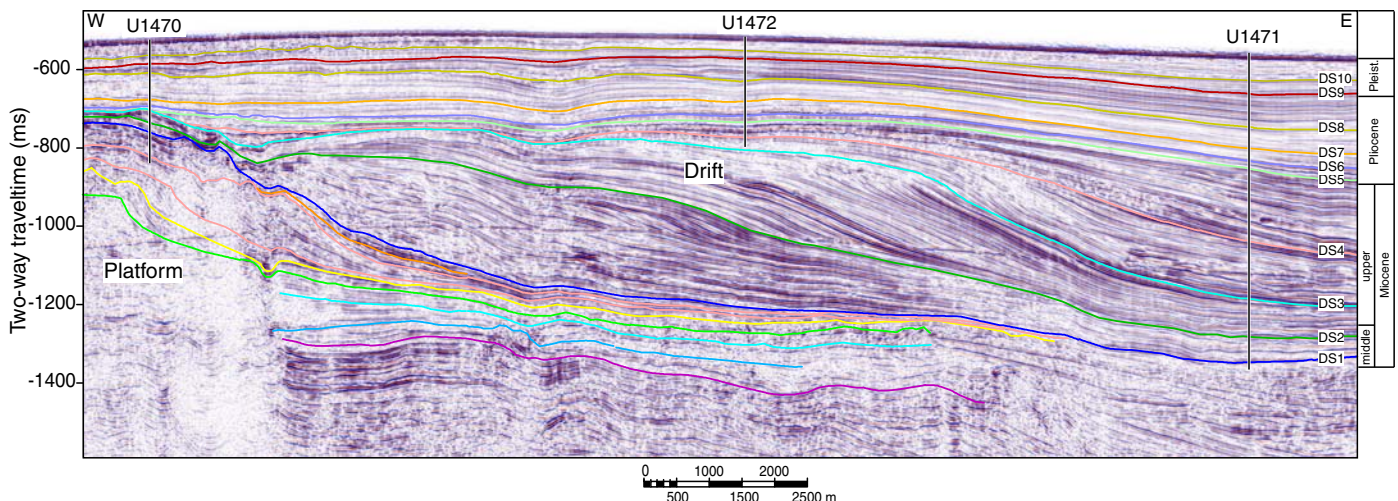


Figure F8. Expedition 359 southern transect with location of sites along seismic Line NEOMA-P62 (vertical exaggeration = 6x) running west–east through southern Kardiva Channel. The position of Site U1472 is projected onto the line; the site is located 400 m north of the line.



mann et al., 2013). Starting with drift sequence (DS) DS6, the opening of a southern gateway introduced northward flow of bottom water into the Inner Sea, leading to deposition of giant elongated drifts at the eastern flank of the basin, filling it from east to west (Betzler et al., 2013a; Lüdmann et al., 2013).

Two additional drowning steps affected the Maldives (Betzler et al., 2009, 2013a). Flat-topped and atoll-shaped banks are interpreted to have drowned quickly, whereas mound-shaped banks are interpreted to have undergone sequential drowning under elevated nutrient fluxes (Betzler et al., 2009), similar to banks described by Zampetti et al. (2004) offshore Malaysia. The drowned banks are elongated parallel to the extension of the Kardiva Channel, which is characterized by throughflow of monsoon-driven surface currents (Betzler et al., 2009). This shape is interpreted as reflecting current control, similar to the recent atolls that are elongated because of the action of waves and currents (Purdy and Bertram, 1993).

Partial drowning steps triggered by currents

An increase in sediment flux into the Indian Ocean occurred around 11 Ma (Rea, 1992; Zheng et al., 2004), and a peak in the sedimentation rates of the Indus Fan took place between 16 and 10 Ma (Clift et al., 2008). Onset and monsoon-intensification steps correlate with the Maldives partial drowning steps (Betzler et al., 2013a). Marine records suggest onset of monsoonal-triggered marine upwelling at ~8.5 Ma (Kroon et al., 1991). It is therefore proposed that monsoon-driven currents and local upwelling shaped the atolls in the past, controlling sediment production and reef growth. Thus, the timing of partial platform drowning and monsoon evolution is linked. Under monsoon conditions, upwelling injected nutrients into surface waters, affecting the carbonate banks (Betzler et al., 2009). This process caused the demise of the barrier reef system, which was replaced by a string of current-shaped relic reefs separated by passages accommodating the throughflow of currents (Betzler et al., 2009, Lüdmann et al., 2013).

Site summaries

Site U1465

Background and objectives

One goal of Expedition 359, in addition to retrieving the record of the Neogene sea level changes in the prograding Kardiva platform and the onset of the monsoon-related currents in drift deposits, was to establish the time and cause of the drowning of the Kardiva platform during the middle Miocene. Platform drowning-related questions were the focus of Site U1465, which is situated above the margin of the drowned Kardiva platform that is overlain by 70 m of sediment. It is the westernmost site of a four-site transect that runs from west to east in the Kardiva Channel. Site U1465 (proposed Site MAL-01A) is located at 4°55.9873'N, 73°0.6786'E, in a water depth of 512.64 m between the Goidhoo and South Maalhosmadulu atolls (Figure F5).

Carbonate platforms are the only depositional system that can cease to exist. The mechanism of the platform demise is usually drowning, but the reason(s) for drowning is still unresolved (Schlager, 1981). Many processes have been proposed, such as global anoxic events, tectonic breakup, and excess nutrients (Arthur and Schlager, 1979; Hallock and Schlager, 1986; Philip and Schlager, 1990; Eberli, 1991). The close relationship between platform drowning and intensification of ocean currents has been proposed for the demise of the Miocene platforms on the Marion Plateau (Isern et al., 2004; John and Mutti, 2005; Eberli et al., 2010).

Betzler et al. (2009, 2013a) and Lüdmann et al. (2013) document partial platform drowning in the Maldives and propose that, in the Maldives, the drowning of the platforms is the combined product of current activity and nutrient supply. Examining the drowning unconformity and the pre- and postdrowning succession in regard to their age, composition, and diagenetic overprint was intended to provide evidence to link drowning directly to the onset of the monsoon-related current system and the concomitant excess nutrient supply from upwelling.

Principal results

At Site U1465, three lithostratigraphic units were identified in the mostly unlithified drift deposits and the underlying lithified platform and slope sediments of the Kardiva platform (Figure F2). Unit I contains unlithified white/light gray to gray-brown and pale yellow packstone to grainstone and, locally, rudstone. The components are planktonic and benthic foraminifers, pteropods, red algae, *Halimeda* plates, bivalves, echinoid fragments and spines, otoliths, and rare solitary corals. Aggregate grains, yellow to brown grains, and black grains occur throughout the entire unit. All lithoclasts and some bioclasts are abraded, which is expected in this drift deposit. The underlying Unit II comprises a shallow-water platform margin facies with diverse coral fauna. The top of Unit II is well-lithified floatstone with corals, red algae, large benthic foraminifers, bivalves, and serpulid fragments that show evidence of exposure and subsequent submarine hardground formation. This thin drowning layer is partly dolomitized and silicified and contains large molds with two generations of dark-colored geopetal infillings that are likely phosphatic (Figure F9). Below this top layer, coral boundstone and floatstone that can be rich in algal nodules alternate. Unit III consists of alternating lithified, very pale brown, coarse-grained dolomitic grainstone to packstone with varying degrees of cementation. The composition is similar to the matrix of the overlying floatstone, but fragments of massive and branching corals decrease and red algae and large benthic foraminifers increase. Other main components are large benthic foraminifers, bivalves, *Halimeda* plates, bryozoa, echinoid spines, gastropods, and abundant bioclasts (Figure F10). Unit III displays all the characteristics of a proximal slope facies, which fits the seismic facies that consists of steeply inclined reflections.

A robust age model was produced by combining the biostratigraphic data of the planktonic foraminifers and calcareous nannofossils in the ~70 m thick drift sediment succession recovered in Hole U1465A above the drowned platform. In the platform and the underlying slope section, the occurrence of planktonic foraminifers and nannofossils was not sufficient for biostratigraphic purposes. The 70 m thick drift sediments range in age from Late Pleistocene to early Pliocene and consist of pelagic faunal elements, fragments, well-preserved echinoderm spine fragments, and fish teeth. All samples contain reworked shallow-water benthic foraminiferal taxa, indicating a range from reefal to middle neritic environments.

Interstitial water (IW) sampling was limited to the uppermost 70 m (i.e., the drift sediments overlying the platform) at Site U1465 by lithification and poor recovery. Concentrations of major anions and cations generally remain constant and close to mean seawater values throughout the sampled interval. For example, Na⁺ and K⁺ concentrations range between 422 and 433 and 10.9 and 11.2 mM, respectively, with no trends visible with increasing depth. Similarly stable values are reflected in Ca²⁺ and Mg²⁺ concentrations, and salinity also remains relatively constant at 34.5–35 throughout the measured interval. This general lack of variation could result from

Figure F9. Geopetal infill (359-U1465A-11X-CC, 5–9 cm). A. Unit II floatstone facies with abundant bioclastic molds, some with geopetal infill (red frame). B. Close-up of geopetal infill in a mold (red frame = contact between original rock and infill). Two different generations of geopetal infill are different brown shades. The uppermost part of the infill displays evidence of bioerosion. C. Close-up of contact between original rock and geopetal infill. Contact surface shows extensive dolomitization marked by sucrosic dolomite. Small planktonic foraminifers (P) floating in a micritic matrix, locally showing porostromate structures, are present in the infill.

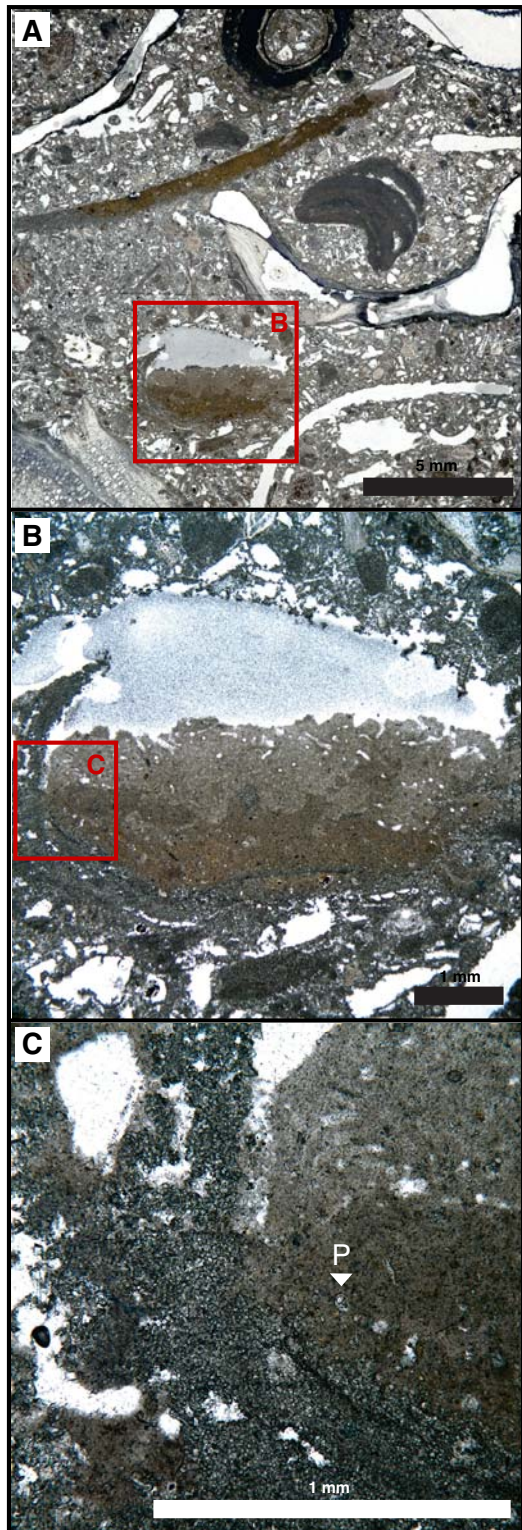
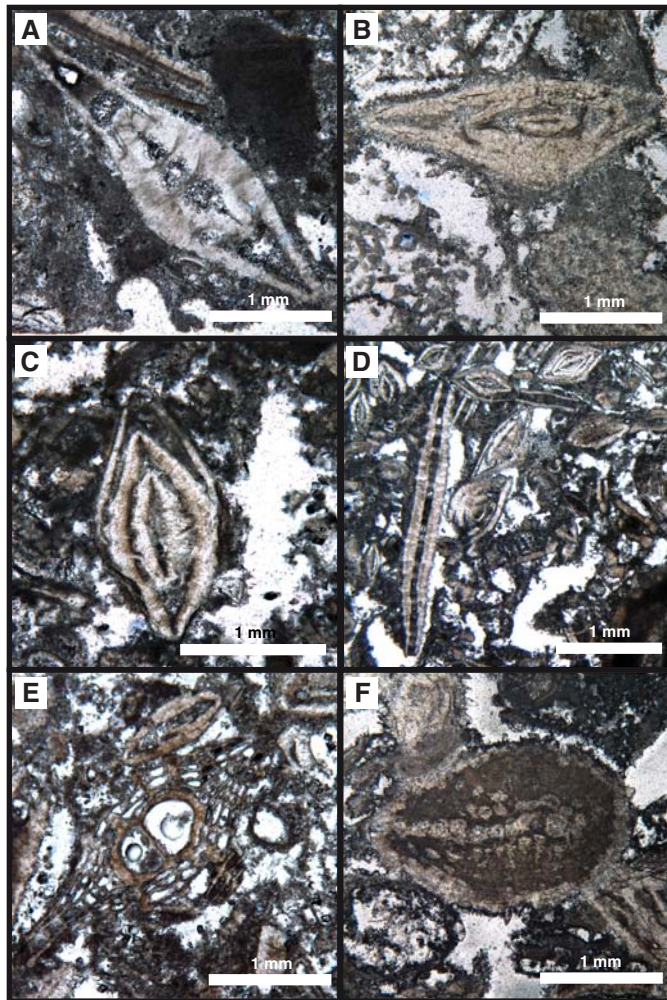


Figure F10. Benthic foraminifers from Units II and III, Hole U1465A. A, B. *Nummulites* sp. (11X-CC, 29–31 cm). C. *Amphistegina* sp. (23R-1, 21–25 cm). D. *Heterostegina* sp. and *Nummulites* sp. (21R-1, 83–86 cm). E. *Lepidocyclus* sp. (21R-1, 83–86 cm). F. *Miogyopsina* sp. (23R-1, 21–25 cm).



three possible situations: no significant diagenesis, high rates of advection, or contamination by seawater.

The lack of geochemical variation contrasts with the mineralogical changes shown by the X-ray diffraction (XRD) data, which reflect carbonate diagenesis during the burial of sediment at Site U1465. Above 45 meters below seafloor (mbsf), the sediment consists of 30%–80% aragonite, 6%–18% high-Mg calcite (HMC), and the remainder low-Mg calcite (LMC). From 45 to 85 mbsf, dolomite is as high as 7%, and aragonite and HMC continue to make up 30%–60% of the sediment (Figure F11). Thus, it is possible that the rate of advection dilutes the geochemical signal of diagenesis in the IW. In the carbonate platform portion, carbonate mineralogy is variable. Below 90 mbsf, the rocks are essentially composed of LMC and dolomite, but below 160 mbsf, aragonite is again present at abundances of <10%. Quartz is often present in the XRD spectra but is never a significant component of the sediment (<1%).

Petrophysical analyses differentiate two physical properties units. The first unit encompasses the loose Pliocene–Pleistocene drift sediments and has high porosities. The lower unit corresponds to the platform carbonates, characterized by higher *P*-wave velocities and higher densities.

Figure F11. Relative concentrations of aragonite, HMC, LMC, dolomite, and quartz measured using XRD, Site U1465. Horizontal dotted line = depth of the drowned platform top as inferred by the disappearance of aragonite.

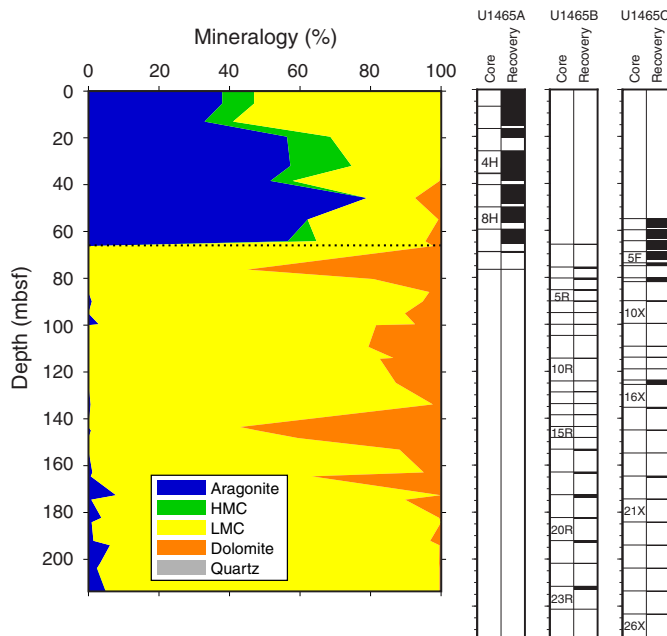
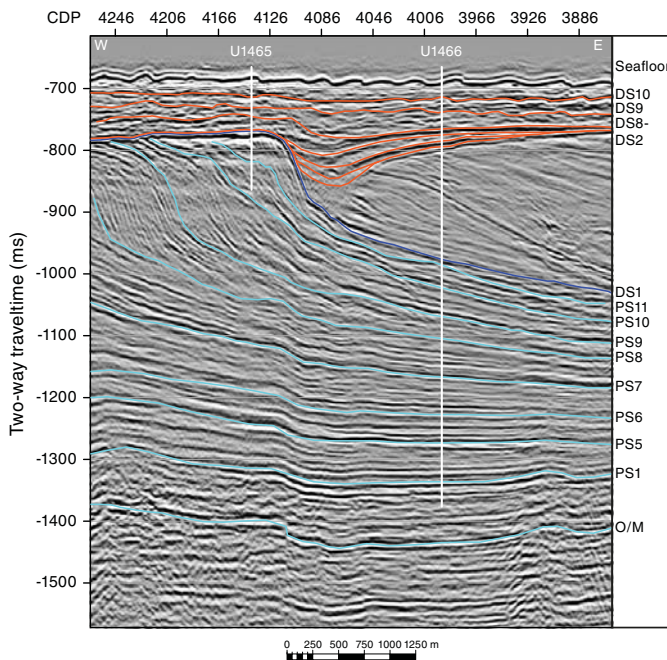


Figure F12. Seismic section showing the drowned Kardiva platform and the onlap and burial by drift sequences, Site U1465. Site U1465 is situated to retrieve the drowned platform carbonates and overlying drift sediments, and Site U1466 is positioned east of the drowned platform edge to retrieve the early Miocene basal sediments, the bottomsets of the prograding platform, the onset and the drift succession. Dark blue line = horizon between platform and drift sequences. O/M = Oligocene/Miocene boundary.



Seismic stratigraphy at Site U1465 shows excellent correlation with lithostratigraphic units (Figure F12). The hiatus separating the platform top from the drifts encompasses DS1–DS6, is biostrati-

graphically dated at Site U1465 as middle Miocene to middle Pliocene (i.e., ~12–3.5 Ma), and corresponds to the boundary between lithostratigraphic Units I and II. The upper part of PS11 at Site U1465 consists of a package of gently basinward-dipping reflections that can be laterally traced over a distance of around 600 m. The lower boundary of the package coincides with sequence boundary PS11, which corresponds to the base of lithostratigraphic Unit II. The deepest hole at Site U1465 (Hole U1465C) was abandoned approximately 9 m above the basal boundary of PS10.

Site U1466

Background and objectives

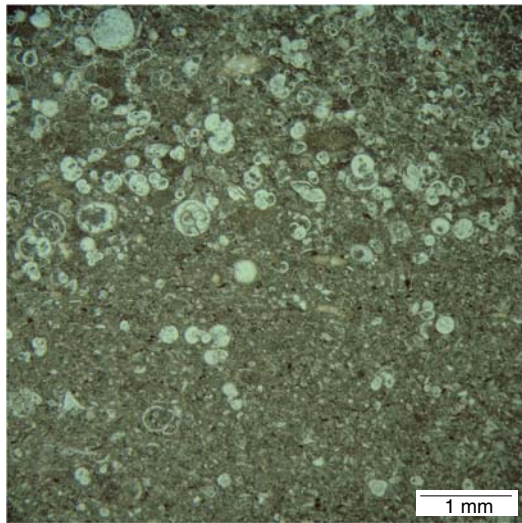
Site U1466 is positioned at 4°55.9880'N, 73°1.6894'E, in a water depth of 518 m 1880 m east of Site U1465 (Figure F5). The site is in front of the last prograding clinoform of the drowned carbonate platform that was the target of Site U1465. In this basal position, a thick drift succession overlays the bottom- and foresets of the drowned Kardiva platform. The pulses of progradation are related to sea level changes, and the overlying drift succession is a current-controlled system that is likely related to the Indian monsoon (Belpolsky and Droxler, 2004a, 2004b; Betzler et al., 2013a, 2013b; Lüdmann et al., 2003). The main goals of this site were (1) to date the transition from the sea level-controlled platform system to the current-controlled drift deposition and (2) to establish an age model for the early and middle Miocene sea level changes in the Indian Ocean and the changes in current evolution since the middle Miocene. The mid-Miocene to recent drift succession contains several sequences caused by fluctuations in the current system (Lüdmann et al., 2013). Dating these sequence boundaries will provide ages of changes in strength and direction of the currents and potentially serve as a proxy for changes in monsoon intensity. Dating of the platform sequence boundaries will provide ages of the sea level lowstands in the Indian Ocean that together with data sets from the Bahamas (ODP Leg 166) and offshore eastern Australia (ODP Legs 133 and 194) will allow testing of the global synchronicity of Neogene sea level changes (Betzler et al., 2000; Eberli et al., 2002, 2010). In addition, the age of the last platform sequence will provide the timing of the platform drowning that potentially is linked to the onset of the current system. Site U1466 cores will also address another objective of Expedition 359: the periplatform sediments deposited at this site offer the opportunity to retrieve a complete record of $\delta^{13}\text{C}$ through the lower and middle Miocene that, together with other Expedition 359 sites, will provide another data set of the carbon isotopic record that is needed to calibrate the periplatform platform margin record against the pelagic record (Swart, 2008).

Principal results

The sedimentary succession at Site U1466 penetrated 803.6 m of lower Miocene to Pleistocene carbonates. This succession consists of a 254 m thick package of drift deposits overlying a 549 m thick succession consisting of the bottomsets and foresets of the middle Miocene prograding platform. Seven lithostratigraphic units were identified in the succession (Figure F2). Lithostratigraphic Unit I through Subunit IVC (0–248.3 mbsf) is from the sediment drift, Subunit IVD through Unit VI (248.3–715.34 mbsf) contains the lithologic record of the prograding tongues of the Kardiva platform, and Unit VII (715.34–803.61 mbsf) is composed of lower Miocene basal carbonates from the Inner Sea.

Unit I is Pleistocene to recent in age and consists of an unlithified coarse-grained grainstone succession. The gray-brown to pale yellow carbonate sand consists almost exclusively of bioclasts, and planktonic foraminifers are the most abundant component, with

Figure F13. Fine-grained packstone with common planktonic foraminifers, a few benthic foraminifers, some mollusk fragments, and abundant bioclasts in a micritic, partially recrystallized, and dolomitic matrix (359-U1466A-50X-CC, 30–33 cm; 317.72 mbsf).



admixtures of benthic foraminifers, pteropods, otoliths, *Halimeda* plates, echinoid spines, bryozoa, and bivalves. The bioclasts are generally broken and show signs of abrasion indicative of current transport.

Unit II is an alternation of unlithified packstone and grainstone, ranging in grain size from very fine to coarse. The main components are planktonic foraminifers and minor benthic foraminifers, pteropods, red algae, *Halimeda* plates, bivalves, echinoid fragments and spines, and otoliths. Aggregate grains, yellow to brown stained grains, and black grains occur throughout the entire unit. Unit III consists of very pale brown medium- to coarse-grained grainstone to packstone that is variably lithified. The main components are planktonic foraminifers, with common to present benthic foraminifers (e.g., *Lepidocyclina*), encrusting red algae, *Halimeda* plates, and bryozoan fragments. Lithification increases downhole to lithified rocks at 99.53 mbsf; below this depth, unlithified and lithified intervals alternate again.

Unit IV consists of four subunits based on the occurrence of textural changes from wackestone to packstone and/or grainstone. The overall lithology is similar throughout the entire unit and consists of skeletal and foraminiferal wackestone to packstone (Figure F13). Unit V is marked by the occurrence of large benthic foraminifers in light gray to light brownish gray, lithified, medium- to coarse-grained dolomitic grainstone and packstone. Unit VI is characterized by a significant increase in the degree of bioturbation that consists of an alternation of decametric intervals of lithified fine- to medium-grained packstones and wackestones with common planktonic and benthic foraminifers, echinoid fragments, and bioclasts. Unit VII consists of an alternation of well-laminated black intervals with massive white chalk and gray-green intervals with moderate to abundant bioturbation (Figure F14). The top of the unit contains intervals with slumps, soft-sediment deformation features, and turbidites.

The age model for Site U1466 (Figure F15) relies on the combination of planktonic foraminifer (Figure F16) and calcareous nannoplankton datums. The estimated sedimentation rate for the Pliocene–Pleistocene sequence is ~1.4 cm/ky. Most of the upper Miocene strata are absent at this site. The hiatus occurs between the

Figure F14. Alternation of black organic-rich and white chalk, Subunit VII B (359-U1446B-56R-1 [top = 789.60 mbsf] and 56R-2).

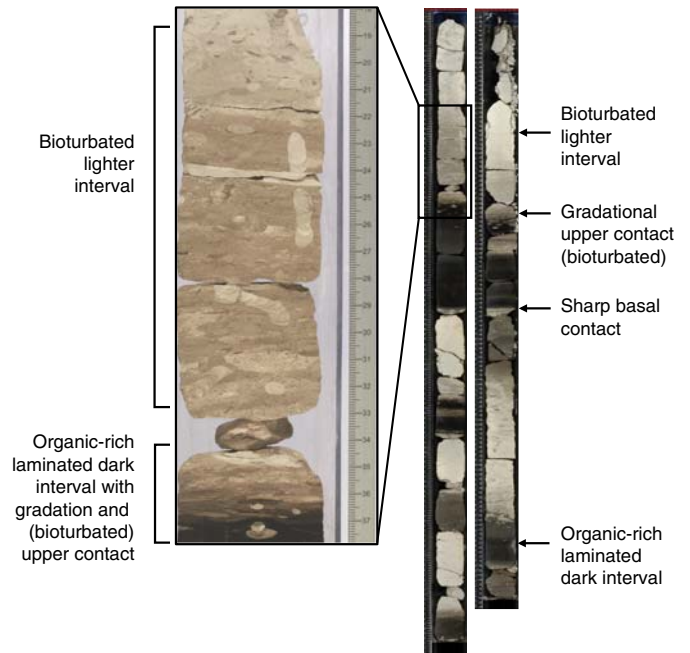


Figure F15. Age-depth profile, Site U1466. L = last occurrence, F = first occurrence. *G.r.p* = *Globigerinoides ruber* pink, *E.h* = *Emiliana huxleyi*, *P.l* = *Pseudemiliana lacunosa*, *G.f* = *Globigerinoides fistulosus*, *D.b* = *Discoaster brouweri*, *D.p* = *Discoaster pentaradiatus*, *G.l* = *Globorotalia limbata*, *D.a* = *Dentoglobigerina altispira*, *S.a* = *Sphenolithus abies*, *D.q* = *Discoaster quinqueramus*, *G.d* = *Globoquadrina dehiscens*, *C.n* = *Coronocyclus nitescens*, *F.f* = *Fohsella fohsi*, *S.h* = *Sphenolithus heteromorphus*, *O.s* = *Orbulina suturalis*, *S.p* = *Sphenolithus pseudoheteromorphus*, *P.k* = *Paragloborotalia kugleri*, *S.d* = *Sphenolithus delphix*.

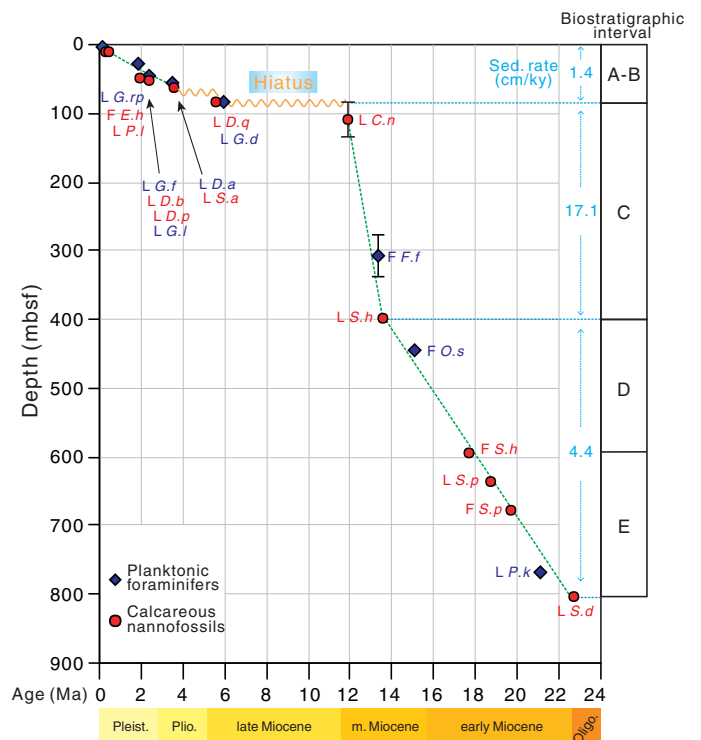
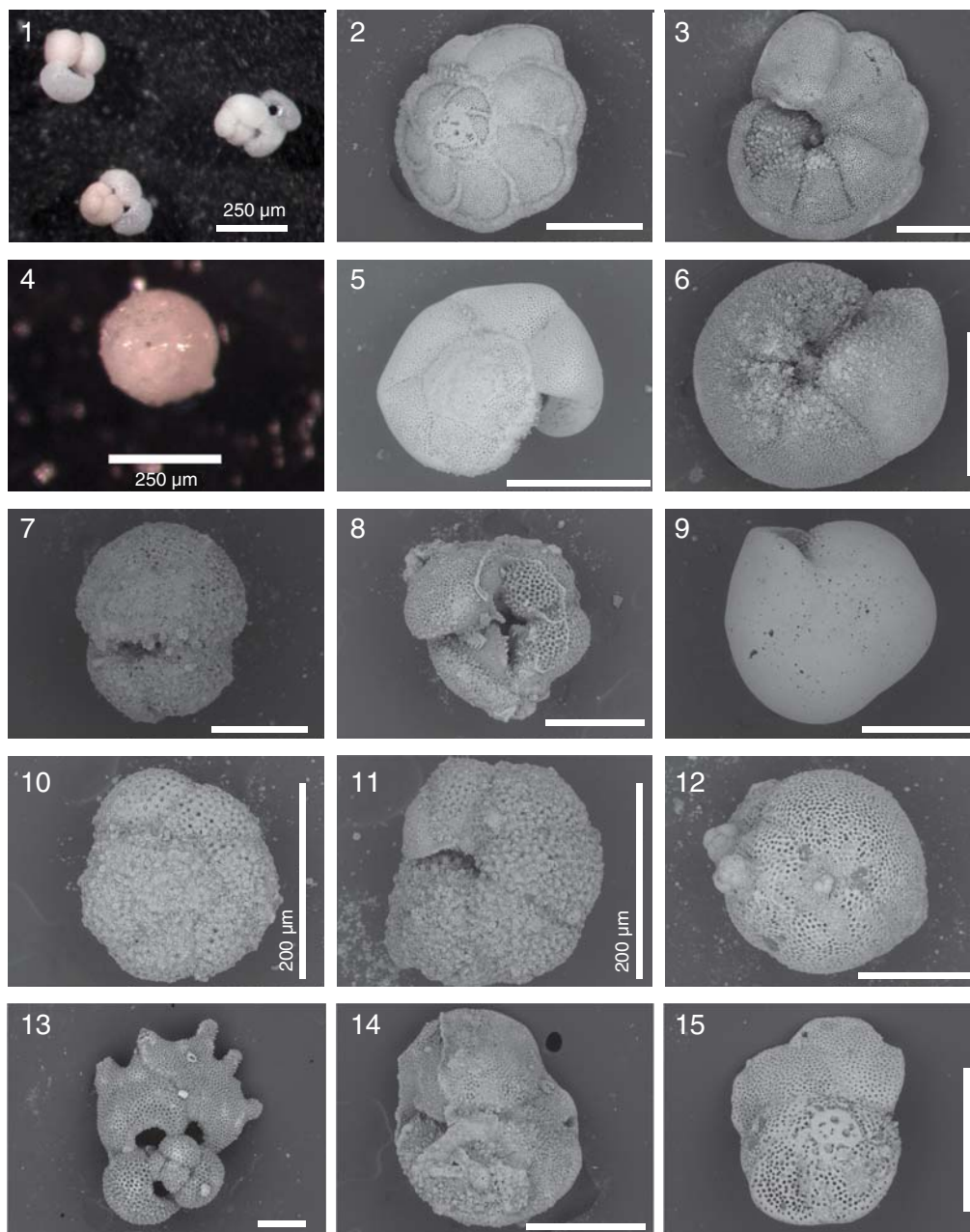


Figure F16. Plate of selected planktonic foraminifers, Site U1466. 1. *Globigerinoides ruber* pink (two specimens on the left) and white (one specimen on the right). 2, 3. *Globorotalia limbata*. 4. *Orbulina suturalis*. 5, 6. *Globorotalia truncatulinoides*. 7. *Praeorbulina sicana*. 8. *Dentoglobigerina altispira*. 9. *Pulleniatina obliquiloculata*. 10, 11. *Paragloborotalia kugleri*. 12. *Globigerinatella insueta*. 13. *Globigerinoides fistulosus*. 14, 15. *Fohsella fohsi*. Scale bars = 250 μm , except where otherwise indicated.



last occurrence (LO) of *Coronocyclus nitescens* (12.12 Ma) and the LO of *Globoquadrina dehiscens* (5.92 Ma). The middle Miocene is divided into two intervals; the basal one presents a moderately high sedimentation rate (~4.4 cm/ky), whereas the upper interval is characterized by a very high sedimentation rate (~17.1 cm/ky). The early Miocene is divided into two intervals according to the preservation of microfossils, although the sedimentation rate does not change through those intervals and remains the same as values in the basal middle Miocene (~4.4 cm/ky).

Pore water studies at Site U1466 in the upper 85 mbsf indicate either relatively low rates of organic matter remineralization or rates of advection by bottom seawater that are faster than the rates

of decomposition of organic matter. The concentration of aragonite remains relatively high throughout the Pleistocene and Pliocene (0–85 mbsf), reflecting either variation in the input from adjacent platforms during changes in sea level or diagenetic change to LMC. Although the hypothesis that aragonite is not being neomorphosed in the upper 85 mbsf is supported by the absence of large increases in the concentration of Sr^{2+} in the pore fluids, the possibility also exists that relative high rates of fluid advection remove evidence of dissolution and precipitation reactions. Below 85 mbsf, aragonite disappears, and at 97.7 mbsf, the sediment contains up to 70% dolomite. Downhole, dolomite content decreases again and up to 20% aragonite is present. Below 320 mbsf, dolomite disappears and is only

barely detectable in trace concentrations through the remainder of the core (Figure F17).

The determination of paleomagnetic polarity based only on inclination data for Site U1466 is extremely weak because of the very low paleolatitude, possible inclination anomalies due to a nondipole field, and poor data quality. Nevertheless, paleomagnetic studies tentatively identify 21 magnetozones using the inclination data. These magnetozones are tentatively attributed to the lower and middle Miocene (C5A–C5E series and C6).

The variability of values in the downhole logs and the measured petrophysical properties (Figures F18, F19) in the pure carbonate strata of Site U1466 reflect changes in diagenesis/lithification and the amount of organic carbon rather than mineral composition. Grain density is similar throughout the entire section. *P*-wave velocity does not correlate well to porosity and displays abrupt increases and decreases downcore, as is typical in pure carbonates. Downhole logging was limited to one run with the modified triple combo tool string to 345 m wireline log depth below seafloor (WSF) because the hole collapsed. In the pure carbonate succession, natural gamma radiation (NGR) is low with two higher peaks related to increased organic carbon content. Resistivity most likely records the degree of cementation, with better-cemented intervals having higher resistivity.

Figure F17. Relative concentrations of aragonite, calcium, dolomite, and quartz measured using XRD, Site U1466. Depths of dolomite peaks are indicated.

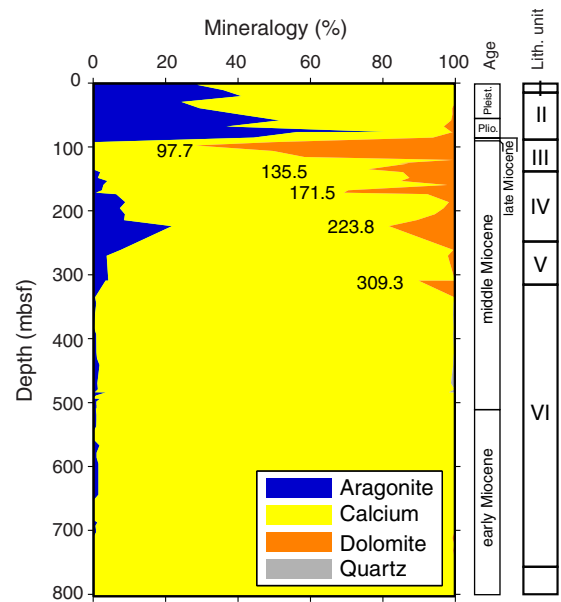


Figure F18. Physical property measurements, Site U1466. As in all sites porosity is very high close to sea surface and although it decreases with depth it remains high to the bottom of the core, ~40%. The constant grain density reflects the consistently high carbonate mineralogy. Bulk density = GRA density from the WRMSL and discrete wet bulk density. Porosity was measured using moisture and density (MAD) mass/volume Method C. PWC = *P*-wave caliper.

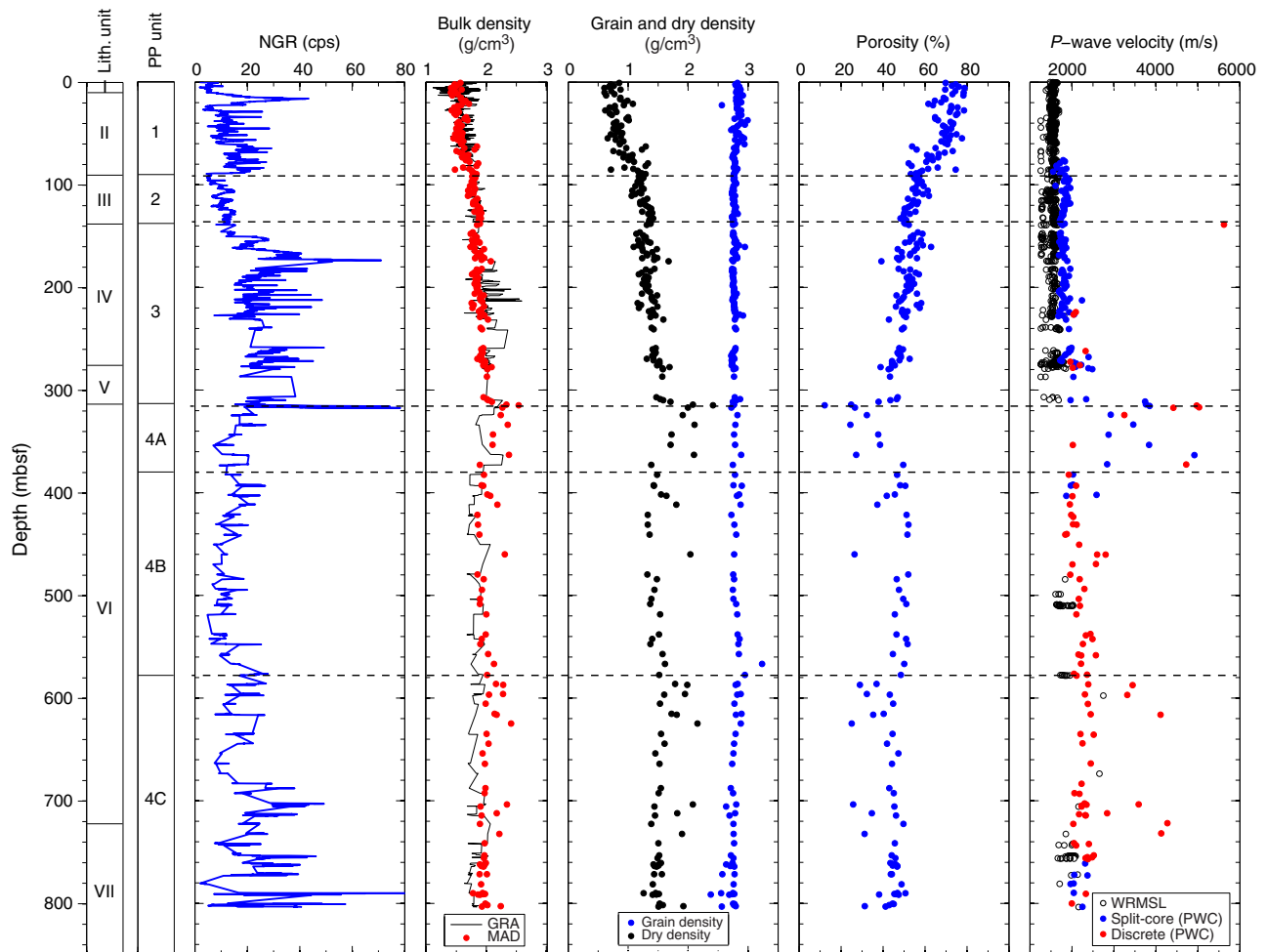
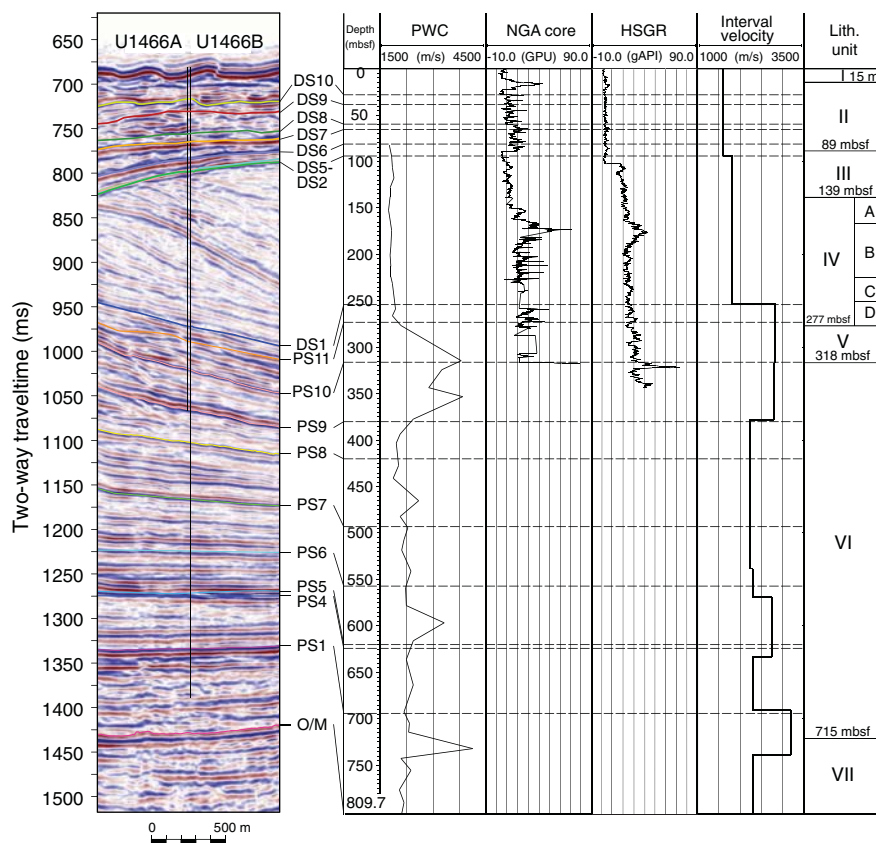


Figure F19. Correlation of seismic, core, and log data, Site U1466. Seismic Line 65 (M74) is shown with bases of platform and drift sequences. PWC = velocity measured on half cores and discrete samples. Interval velocity = model for time-depth conversion.



The correlation of the lithostratigraphy and age model from biostratigraphy to the seismic stratigraphy confirms and refines the predrilling interpretation (Figure F19). The continuous seismic reflections of the distal clinoforms of the sea level-controlled Kardiva platform are lithologically a regular alternation of intervals of lithified fine- to medium-grained packstones and wackestones. These alternations are most likely the result of high-frequency sea level changes. The onset of the drift succession is recorded by a change in seismic and lithologic facies. Seismic reflection amplitudes decrease, and the lithology is dominated by coarse-grained packstone and grainstone, reflecting a current-dominated sedimentation pattern.

Site U1467

Background and objectives

Site U1467 is the easternmost site drilled in the Inner Sea of the Maldives during Expedition 359. It is located at 4°51.0274'N, 73°17.0223'E, at a water depth of 487.4 m (Figure F5). This site is positioned on a 630 m thick succession of drift deposits lining the southern flank of the Kardiva Channel. The main objectives were (1) to precisely date the onset of the drift deposition and to constrain the timing of sequence boundaries in the drift succession; (2) to analyze the cyclostratigraphy of carbonate drift deposits, providing reconstructions of changes in the current regime and monsoon cyclicality; and (3) to recover an undisturbed sedimentary sequence for further paleoceanographic studies.

The mid-Miocene to recent drift succession contains several sequences that are likely caused by fluctuations in the current system

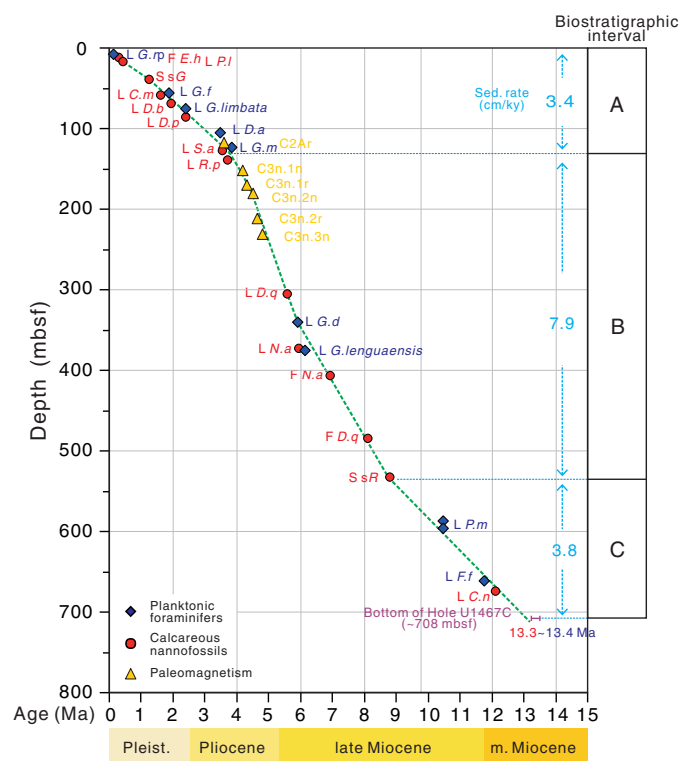
flowing through the Kardiva Channel. Dating these sequence boundaries will provide the ages of changes in strength and direction of the currents. Further linking of these physical stratigraphic data with postexpedition sedimentological and geochemical data will address the question of changes in the monsoon intensity (Kroon et al., 1991; Prell et al., 1992; Clift et al., 2008; Gupta et al., 2015). Moreover, the periplatform sediments deposited at this site offer the opportunity to retrieve a complete record of $\delta^{13}\text{C}$ through the middle Miocene that, together with the other Expedition 359 sites, will provide another data set of the carbon isotopic record that is needed to calibrate the periplatform record against the pelagic record.

Principal results

Five holes were drilled at Site U1467, one of them (Hole U1467E) as a dedicated logging hole. The sediment recovered at Site U1467 is a fine-grained succession of wackestone to packstone. Compositional changes are minor, but alternation of lighter and darker intervals of variable thickness persists downhole, even through the increasing degree of lithification to approximately 640 mbsf. Six lithostratigraphic units were differentiated (Figure F2).

Unit I (0–110.0 mbsf) consists of unlithified, foraminifer-rich wackestone to packstone with a predominance of very fine- to fine-grained wackestone. The unit is characterized by thick (30–100 cm) to very thick (>100 cm) intervals defined by color changes ranging from light gray to grayish brown. The dark colored intervals correlate with low lightness L^* reflectance values and display an inverse

Figure F20. Age-depth profile, Site U1467. The age constraint for the base of the recovered sediments from <13.3–13.4 Ma is based on several reliable events which must occur below the base of Hole U1647C. The green dotted correlation line and sedimentation rates are based on biostratigraphic data alone, and magnetostratigraphic data has been added to show good coherence between these data sources. Plotted paleomagnetic events are chron tops. L = last occurrence, F = first occurrence. *G.r.p* = *Globigerinoides ruber* pink, *E.h* = *Emiliania huxleyi*, *P.l* = *Pseudoemiliania lacunosa*, *S.sG* = Start small *Gephyrocapsa* event, *C.m* = *Calcidiscus macintyre*, *G.f* = *Globigerinoides fistulosus*, *D.b* = *Discoaster brouweri*, *G.limbata* = *Globorotalia limbata*, *D.p* = *Discoaster pentaradiatus*, *D.a* = *Dentoglobigerina altispira*, *S.a* = *Sphenolithus abies*, *G.m* = *Globorotalia margaritae*, *R.p* = *Reticulofenestra pseudumbilicus*, *D.q* = *Discoaster quinqueramus*, *G.d* = *Globoquadrina dehiscens*, *N.a* = *Nickolithus amplifucus*, *G.lenguaensis* = *Globorotalia lenguaensis*, *S.sR* = Start small *Reticulofenestra* event, *P.m* = *Paragloborotalia mayeri*, *F.f* = *Fohsella fohsi*, *C.n* = *Coronocyclus nitescens*.

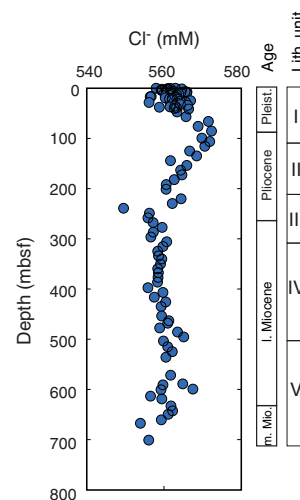


relationship with NGR trends, with higher NGR (counts/s) observed in the darker intervals.

Unit II (110–215 mbsf) is defined by interlayered unlithified and partially lithified planktonic foraminifer-rich wackestone and mudstone with pteropods and particulate organic matter. The matrix of the sediment contains calcareous nannofossils and sponge spicules. Celestine is common as nodules and layers up to 3 cm thick and as disseminated crystals in the fine fraction.

Unit III (215–303 mbsf) consists of partially lithified very fine grained mudstone to wackestone with a dominance of wackestone. The unit also has thick to very thick packages with color changes, from light gray to light olive-gray and light brownish gray. The sediment contains abundant planktonic foraminifers; echinoid spines and sponge spicules are common, but benthic foraminifers are rare. Celestine nodules and fragments, bioclasts, and particulate organic matter are common, especially in the darker intervals. Bioturbation is common with *Thalassinoides*, *Planolites*, *Palaeophycus*, and pos-

Figure F21. Concentrations of Cl⁻, Holes U1467A–U1467C. The excursion at 100 mbsf may be a relict signal related to the last glacial period, when salinity was altered as a result of Northern Hemisphere glaciation.



sibly *Zoophycos*. Traces appear better developed in the darker colored intervals.

The deposits of Unit IV (303–498.5 mbsf) are lithified, very fine to medium-grained, planktonic foraminifer-rich wackestone to packstone. As with previous units, particulate organic matter is present and changes in abundance, which is linked to color variations from light gray to light brownish gray and pale yellow with gradational and commonly bioturbated contacts. Ichnofauna consist of *Thalassinoides*, *Planolites*, *Zoophycos*, *Chondrites*, and *Palaeophycus*.

Unit V (498.5–607 mbsf) still consists of planktonic foraminifer-rich wackestone to packstone with alternating light and dark intervals, but lithostratigraphic Unit VI below 607 mbsf lacks dark layers within the fine-grained wackestone.

Biostratigraphic analyses show an apparently continuous succession of Holocene to middle Miocene age recovered at Site U1467 (Figure F20) that is divided into three intervals. The Pleistocene and upper Pliocene extends from the seafloor to ~130 mbsf. Throughout this interval, planktonic foraminifers are well preserved, whereas benthic foraminifers and calcareous nannofossils are well preserved at the top but moderately well preserved below 40 mbsf. The lower Pliocene and much of the upper Miocene extends from ~130 to 540 mbsf. Preservation throughout this thick interval is poor to moderate for all microfossils, except in the deepest core in this interval (Core 359-U1467B-69X), from which very well preserved nannofossils were recovered from a few darker, probably clay-rich levels. The late Miocene and later part of the middle Miocene extends from 540 to 714 mbsf.

Decreases in SO₄²⁻ concentrations and alkalinity in the interstitial fluid geochemistry from Site U1467 indicate that significant remineralization of organic material occurred below 50 mbsf. An odor of H₂S was also noted upon core recovery and squeezing of the whole-round samples, suggesting that bacterial sulfate reduction probably accounts for the observed trend. As large amounts of NH₄⁺ are released during decomposition of sedimentary organic matter, a negative correlation between SO₄²⁻ and NH₄⁺ is also related to the oxidation of organic matter. Cl⁻ increases from the sediment surface to around 100 mbsf (Figure F21) and may be related to the last gla-

cial period, when salinity was altered as a result of Northern Hemisphere glaciation.

Site U1467 sediments contain up to 60% aragonite in the upper 50 m of the core. Below 50 mbsf, aragonite content decreases to less than 10%–15% and drops to less than 10% by 500 mbsf. This decrease is interpreted to reflect aragonite dissolution, based on increases of Sr^{2+} concentrations in the pore fluids. Deposits are again richer in aragonite between 500 mbsf and the bottom of the hole; Sr^{2+} concentrations of the pore fluids decrease slightly in this interval, whereas Li^+ concentrations increase. There are several occurrences of celestine (SrSO_4) between 163 and 393 mbsf, indicating that the pore water concentrations of Sr^{2+} and SO_4^{2-} attain supersaturation with respect to this mineral.

Organic carbon content in Site U1467 sediments fluctuates between 0 and 12 wt%, with the samples richest in organic carbon at 89, 112, and 168 mbsf. Methane remains at concentrations between 1.6 and 12.0 ppmv, increasing slightly from the surface to 300 mbsf and then remaining mostly stable around 5 ppmv with some scattering of values. Ethane is only present in measurable quantities (~ 1 ppmv) between 249 and 277 mbsf and at 324, 580, and 706 mbsf.

Natural remanent magnetization (NRM) analysis at Site U1467 was only possible on limited core sections because of pervasive contamination, presumably from rust in the drill pipe that affected the first two to three sections of every core, despite cleaning the drill pipe interior while in Hole U1467C. Nevertheless, a series of magnetozones between ~ 100 and 200 mbsf in Hole U1467C and between 195 and 255 mbsf in Hole U1467B were identified and interpreted as Chrons C2Ar to C3n.3n (Figure F20). Another series of possible normal and reversed polarity intervals based only on the analysis of inclinations, which are less than 20° and consistent with the paleolatitude for this site, was recognized between 580 and 714 mbsf in Hole U1467C (Cores 24X–37X) and interpreted to be Chrons C5n.2n to C5An.2n.

The physical properties of the sediment reflect the rather monotonous nature of the lithologic succession at Site U1467, which is mainly characterized by the changes of color from darker to lighter intervals in generally fine-grained bioturbated wackestone. Below 465 mbsf, where the formation is more lithified, density and velocity increase significantly and show large variations. High-frequency fluctuations in NGR also follow color variations, which are likely produced by small admixtures of organic material (dark color) and more early marine cements (light color). In addition, NGR data display five longer term variations that loosely follow the lithostratigraphic units. Magnetic susceptibility is low throughout the entire core.

In the dedicated logging Hole U1467E, three tool strings were deployed: the triple combo, Versatile Seismic Imager (VSI), and Formation MicroScanner (FMS)-sonic tool strings. The VSI tool string recorded good sonic waveforms at 13 stations at a 50 m interval. After shore-based processing, logging data were analyzed and divided into four logging units. Logging unit boundaries correlate with some of the lithostratigraphic units (Figure F22). Most variations in the downhole logs are seen in the gamma ray values, triggered by differences in the uranium content, which correlate to variations in the amount of organic matter as revealed by smear slide analysis. VSP data and sonic velocity logs helped to establish the conversion between depth and two-way traveltime (TWT) and thus allowed us to exactly tie in seismic and core data.

Stratigraphic correlation using available biostratigraphic and paleomagnetic age control points allowed us to refine and establish

a precise age model for Site U1467 that correlates the different physical property measurements and the downhole logging data. A composite depth scale and splice at Site U1467 were constructed from 0.0 to 220.25 m core composite depth below seafloor (CCSF-D) (from the “mudline” in Hole U1467C to the bottom of Core 359-U1467B-22H).

In the seismic profiles, the drift sequences at Site U1467 are represented by well-stratified, nearly horizontal, low- to medium-amplitude reflections and in the lower part by a succession of strong reflections. Site U1467 is located in a basinal position where all sequence boundaries appear as continuous parallel reflections, which are the correlative conformities to the unconformities along the basin margin that define the sequence boundaries. The thickness of the drift sequences varies from 24.5 m (DS7) to 104 m (DS6) and 173 m (DS4). Starting with DS1–DS3, the depocenter was situated at the western basin margin and dominated by southward bottom water inflow from the northeast Kardiva Channel and inflow from the newly opened northwest Kardiva Channel. DS4–DS7 mark the gradual eastward shift of the depocenters. The uppermost sequences (DS8–DS9) exhibit a more uniform thickness throughout the Inner Sea of the Maldives.

Site U1468

Background and objectives

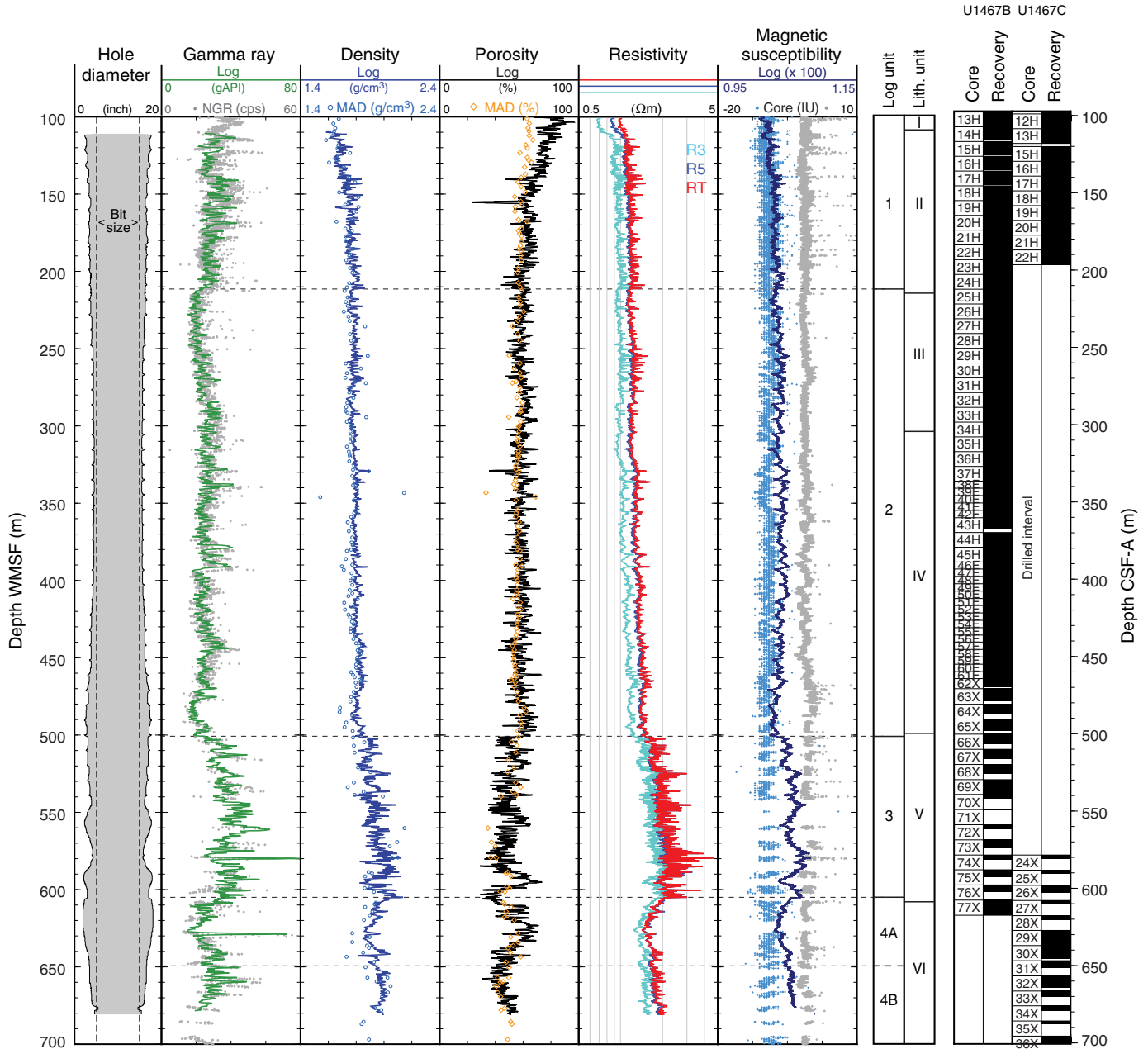
Site U1468 is located in the Kardiva Channel in the Inner Sea at $4^\circ 55.9823' \text{N}$, $073^\circ 4.2834' \text{E}$. This site is the easternmost site of the northern transect, 4.8 km east of Site U1466 (Figure F5). At Site U1468, seismic profiles indicate a succession with the Oligocene/Miocene boundary at 710.5 ms TWT followed by the basinal to lower slope deposits of the lower–middle Miocene Kardiva carbonate platform. The base of the overlying drift succession (reflection DS1) is a gently basinward-dipping horizon. The drift itself is 431 ms TWT thick, which equals 433 m. The modern current-swept seafloor is at 521.45 m water depth.

Site U1468, together with Site U1466, is a key site (1) to constrain the timing of the platform to drift turnover, (2) to date the sequence boundaries of the Kardiva platform, and (3) to reconstruct the platform evolution from the Oligocene/Miocene boundary onward. With regard to the drift sequences, the position of Site U1468 was chosen because it bears an extended thickness of the DS1 succession and a greater thickness of DS2 compared to the succession at Site U1466. Additionally, it allows us to study the proximal to distal depositional trend in the drift package. Because the sequences of the mid-Miocene drift succession are likely to be determined by fluctuations of the bottom-current regime (Lüdmann et al., 2013), dating such variations and understanding the drift facies will help to address the paleoceanographic objective of the expedition to link the changes of the Maldives current regime to global Neogene ocean circulation. The succession recovered at Site U1468 also provides the opportunity to retrieve a complete record of $\delta^{13}\text{C}$ variations in periplatform carbonates through the lower and middle Miocene for establishing the carbon isotopic record needed to calibrate this hemipelagic record against the pelagic record.

Principal results

Two holes were drilled at Site U1468. Hole U1468A cored 873.7 m of carbonates (with 53% recovery) using a combination of the advanced piston corer (APC), half-length APC (HLAPC), and extended core barrel (XCB) coring systems. Hole U1468B was drilled as a dedicated logging hole with the rotary core barrel (RCB) system to 874.7 mbsf. Sediments from a variety of depositional settings

Figure F22. Triple combo logs, Hole U1467E. Note that downhole logs are on the logging depth scale, whereas the natural gamma ray (NGR), density and porosity (MAD), and magnetic susceptibility (WRMSL = gray dots; point magnetic susceptibility [MSP] = blue dots) core data from Holes U1467B and U1467C and core recovery are on the core depth scale. HRLA: R3 = medium resistivity, R5 = deepest resistivity, RT = true resistivity, modeled from all depths of investigation.



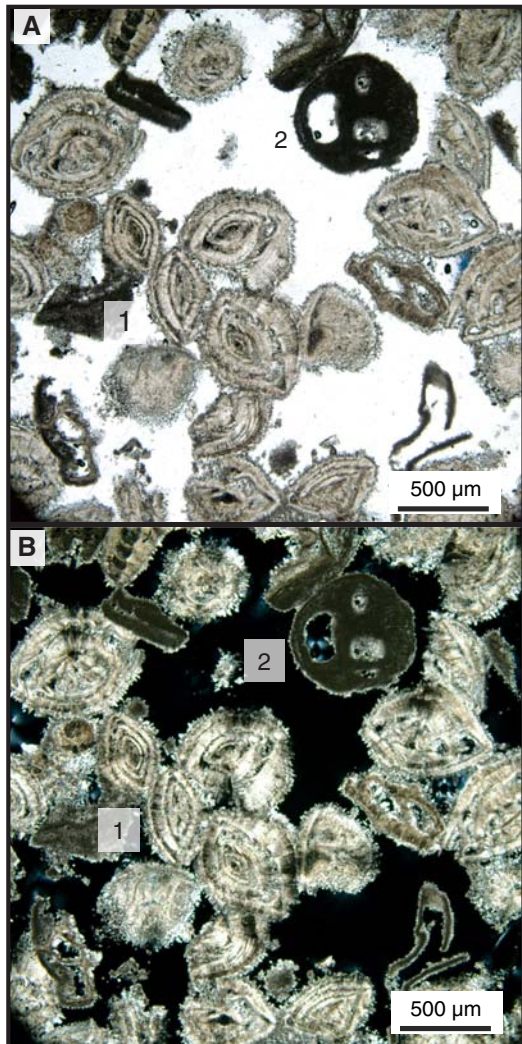
were recovered at Site U1468. The top formed a drift package that comprises lithostratigraphic Units I–IV, and the Miocene distal slope and the basinal deposits of the Kardiva platform form lithostratigraphic Unit V (Figure F2). A restricted basin environment defines lithostratigraphic Unit VI. Lithostratigraphic Units VII and VIII are shallow-water deposits.

Unit I (0–45.7 mbsf) is dominated by light gray and pale yellow to white un lithified to partially lithified packstone to grainstone. Deposits are rich in planktonic foraminifers and contain abundant benthic foraminifers, ostracods, pteropod fragments, *Halimeda*

fragments, mollusk fragments, echinoid fragments and spines, otoliths, fish remains, and very rare bryozoans. Foraminifers and bioclasts are well preserved with aggregate grains, organic matter, and yellow- to brown-stained lithoclasts. The fine fraction contains aragonite needles (<5 μm), calcite crystals (5–10 μm), and calcareous nannofossils (coccoliths). Variations in grain size and texture, in particular the gradual change from packstone to grainstone layers, are interpreted to be the result of changing current strength.

Unit II (45.7–192.4 mbsf) mainly consists of un lithified to partially lithified rudstone to wackestone with abundant to frequent

Figure F23. *Amphistegina* sp. grainstone (359-U1468A-7H-2, 48–50 cm): 1 = *Amphistegina* sp., 2 = red algal debris. Fossils and clasts are cemented together by sparry cements. A. Plane-polarized light (PPL). B. Cross-polarized light (XPL).

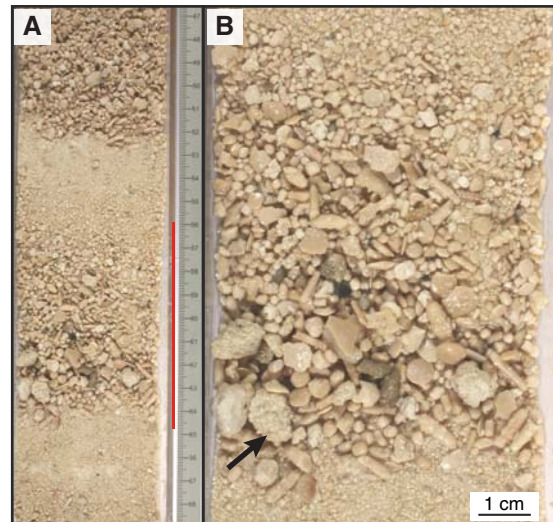


large benthic foraminifers (Figure F23). The matrix throughout the entire unit contains abundant calcite crystals and very rare dolomite rhombs and calcareous nannofossils. Rudstone layers containing rip-up clasts, other small lithoclasts, echinoid spines and fragments, and other large bioclasts often form the base of graded beds that have a slight erosional base and fine upward to a fine-grained grainstone (Figure F24).

Unit III (192.4–296.4 mbsf) is a light brownish gray to light gray wackestone succession with intercalations of packstone. This unit is characterized by the reappearance of planktonic foraminifers and the disappearance of large benthic foraminifers. Intraclasts are common, indicating early marine cementation and reworking. Most bioclasts are heavily overgrown with dogtooth calcite crystals. The matrix contains abundant calcite crystals, whereas sponge spicules are minimally present within the fine matrix. Calcareous nannofossils are extremely rare to absent.

Unit IV (296.4–427.7 mbsf) consists of lithified packstone to wackestone. Components in this unit include bioclastic fragments, as well as planktonic and benthic foraminifers that are severely overgrown by calcite cements. The degree of bioturbation in this

Figure F24. Unit II, Hole U1468A. A. Fining-upward layers from very coarse grained rudstone to fine-grained packstone with an erosional surface at each layer (17F-1, 47–68 cm). The top of this section is the Subunit IIA/IIB boundary. B. Close-up of very coarse grained rudstone (17F-1, 56–65 cm; red line in A) showing large components (≈ 1 cm) such as rip-up clasts (arrow), large benthic foraminifers, echinoid spines, and extraclasts.



unit allows the identification of several ichnotaxa, including *Thalassinoides*, *Palaeophycus*, *Planolites*, and *Chondrites*. Occasionally, some burrows are silicified.

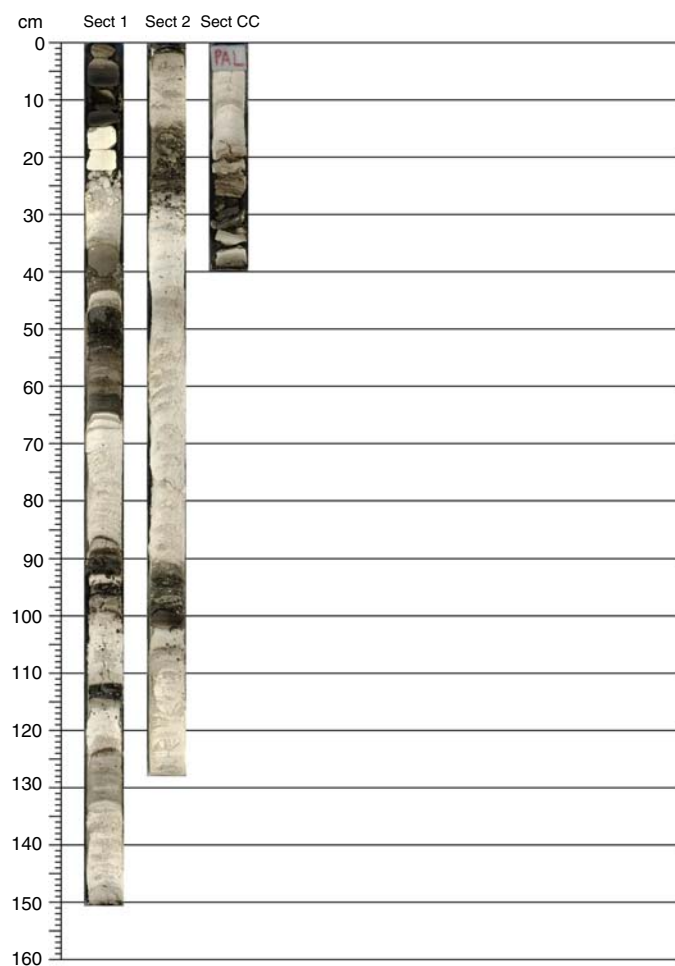
Massive wackestone makes up Unit V (427.7–728.6 mbsf). Throughout the unit are alternations of light and dark intervals; the darker color is linked to a higher abundance of organic material. The main components in this unit are planktonic foraminifers, with benthic foraminifers, mollusk fragments, and bioclast fragments. The components found have calcite cement overgrowth. The well-preserved ichnotaxa identified within this unit include *Thalassinoides*, *Teichichnus*, *Asterosoma*, *Phycosiphon*, *Zoophycos*, *Palaeophycus*, *Planolites*, and *Chondrites*.

Unit VI (728.6–815.9 mbsf) is a wackestone to packstone succession that consists of light gray chalk with intercalations of dark gray to black layers with abundant organic matter (Figure F25). Planktonic foraminifers are abundant, and the rock matrix consists of calcareous nannofossils. Unit VII is layered wackestone with floatstone intercalations containing large benthic foraminifers *Amphistegina*, *Lepidocyclina*, *Cycloclypeus*, and *Miogyopsina*.

Unit VIII forms the lowest part of the cored succession at Site U1468. It is densely cemented limestone that contains abundant shallow-water biota such small and large benthic foraminifers, *Halimeda* plates, bivalve fragments, and bryozoan and coral fragments.

Biostratigraphic analysis of the microflora and microfauna allowed us to divide the succession into four intervals. Interval A reaches to ~ 45 mbsf and ranges in age from the late Pliocene to Quaternary. The lower part of the Pliocene is missing. Interval B extends from about 45 to 429 mbsf. It comprises middle to late Miocene calcareous microfossils, which are generally sparse and poorly preserved throughout the succession. One sample at 40.59 mbsf contains a few late Miocene to Pliocene–Pleistocene specimens of planktonic foraminifers mixed with abundant abraded and recrystallized large foraminifers. The base of biostratigraphic interval B corresponds to the base of the drift sequence as determined by seismic stratigraphy and lithostratigraphy. Interval C encompasses the middle Miocene to upper Oligocene between 447.3 and 827.4 mbsf

Figure F25. Light–dark alternations in coccolith-rich lower Miocene deposits (359-U1468A-99X).



with abundant and moderately to well-preserved calcareous nannoplankton. The lowest interval D contains mainly large benthic foraminifers derived from the foreereef environment.

Geochemical analyses revealed minimal changes in the $\text{SO}_4^{2-}/\text{Cl}^-$ ratio and alkalinity of the interstitial fluids in the uppermost 200 m. Below 200 mbsf, a net decrease in the concentration of SO_4^{2-} is caused by bacterial sulfate reduction. The aragonite concentration in the sediments remains between 20% and 40% throughout the uppermost 50 m, reflecting variations in input rather than diagenetic change to LMC. The sudden loss in aragonite below ~50 mbsf suggests a period of exposure to fluids that caused partial dolomitization. Neomorphism of the sediments to LMC and some limited amount of dolomitization is indicated by the rapid increase in the $\text{Sr}^{2+}/\text{Ca}^{2+}$ ratio of the pore water below 200 mbsf. Although dolomite formation is supported by the decline in the Mg/Ca ratio of the pore fluid, the present dolomite formation indicated by pore water data is not responsible for the up to 25% dolomite found in the sediments. This indicates that dolomite must have formed during earlier time periods in a different fluid regime than observed at the present. The large increase in Sr^{2+} in Unit III causes the pore fluids to attain saturation with respect to SrSO_4 and precipitation of celestine, detected by XRD.

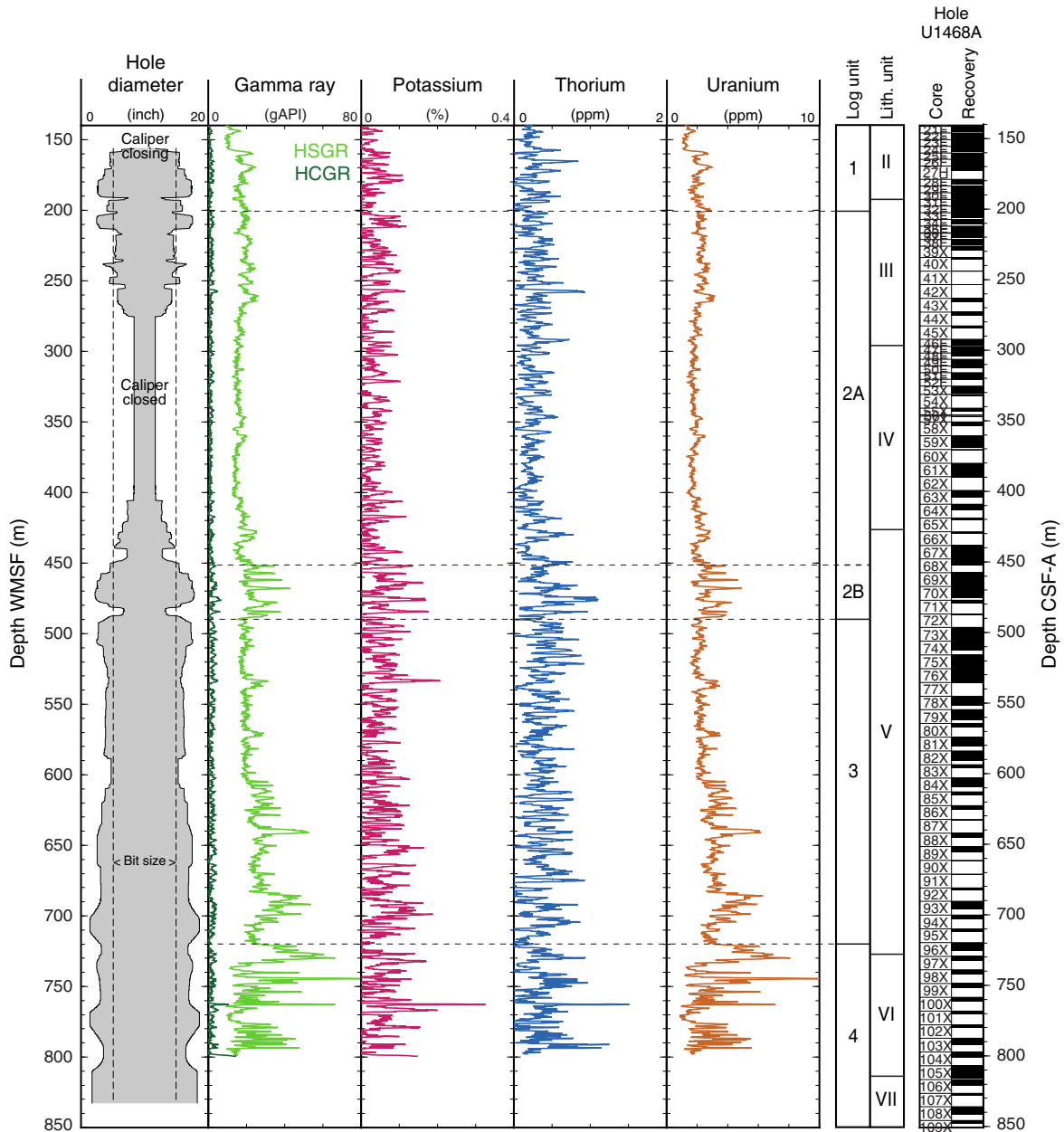
The influence of noncarbonate components on pore water chemistry can be seen between 450 and 500 mbsf, where the carbonate content of the sediments decreases to ~80%. Here, K^+ in the pore waters increases slightly. Increased Fe in the sediments and the marked increase in the Mn/Ca ratio below this depth clearly indicate the significance of this transition, which is reflected in a significant reduction in the rate of sedimentation as indicated by biostratigraphic data.

Paleomagnetic analyses show contamination of the core sediment with highly magnetic material. This is unambiguously shown by the typical pattern of NRM intensity that decreases from the upper to lower part of each core by 3 or 4 orders of magnitude. APC and HLAPC cores drilled in the upper part of Hole U1468A seem more affected by this problem compared to XCB cores drilled in the deepest part of the same hole. The distribution of inclinations, despite the large scatter, has a single mode at 0° , suggesting that Site U1468 crossed the Equator during the early Miocene.

The strata at this site can be divided into five physical properties units. NGR has the most variability and basically defines the physical properties units, but other properties also contribute. For example, in physical properties Unit 1 (0–50 mbsf), bulk density is low and porosity is high. At 50 mbsf, they shift abruptly to higher (density) and lower (porosity) values, and subsequently they only show a slight increase and decrease, respectively, to the bottom of the hole. Porosity remains very high even to great burial depths, with over 50% porosity at 800 mbsf. Likewise, velocity only displays a slight overall increase in physical properties Units 2–5 to about 2400 m/s, but high values of up to ~4000 m/s are measured in the more lithified beds. A velocity inversion occurs in physical properties Unit 4 produced by the chalk interval of lithostratigraphic Unit VII. Color reflectance quantifies the observed cyclic dark–light alternations in the rock but also captures the overall darker tones of lithostratigraphic Units II and IV.

A dedicated logging hole was drilled at Site U1468 to ensure a complete set of downhole measurements. During the first logging run with the triple combo tool string, however, wireline tension increased at 485 m WSF and caliper measurements indicated a narrow borehole less than 7 inches in diameter. These collapsing hole conditions persisted to 280 m WSF, above which the logging run could be completed. No additional logging tool strings were run. In the narrow interval of the collapsing hole, data quality was reduced but the lower and upper portion yielded good data. Based on the electrical resistivity and gamma ray logs, four logging units were identified. Logging Unit 1 extends from the base of the drill pipe to 201 m wireline log matched depth below seafloor (WMSF) and is characterized by low gamma ray and resistivity values, both with low to moderate amplitude variability except for two peaks around 190 and 200 m WSF. Logging Unit 1 correlates mostly with lithostratigraphic Unit II, which in the logged interval displays an overall coarsening-upward trend and textures from mudstone to packstone at the base and grainstone to rudstone at the top. In logging Unit 2 (201–490 m WSF), the character of the resistivity changes with alternations of lower and higher resistivity over intervals of meters to tens of meters. The gamma ray log is nearly flat, except at the base of the unit between 450 and 490 m WSF. This logging unit corresponds to lithostratigraphic Units III and IV and part of V. Units III and IV correspond to the drift sediments of DS1 (Figure F26), which is composed of wackestone with some packstone intervals (Unit III) and lithified packstone (Unit IV). Intervals of higher

Figure F26. Triple combo logs, Hole U1468B. Note that downhole logs are on the logging depth scale, and NGR and magnetic susceptibility (WRMSL and MSP) core data from Hole U1466A and core recovery are on the core depth scale. HSGR = standard (total) gamma ray, GR EDTC = total gamma ray from EDTC. HRLA: R3 = medium resistivity, R5 = deepest resistivity, RT = true resistivity, modeled from all depths of investigation.



gamma ray and corresponding resistivity variations at the base of logging Unit 2, from 450 to 490 m WSF, capture alternations of sub-meter to multiple meter scale light and dark intervals deposited at the distal bottomsets of the prograding Kardiva platform that are characterized by the alternations of darker and lighter packstones to wackestones. The resistivity log reflects this rather uniform lithology with low variability values that slightly increase with depth. The gamma ray log displays more variability from low to moderate amplitude and also increases with depth. These variations in the gamma ray signature are mostly the result of uranium variations that are likely related to changes in the organic material that varies from the dark (high) to light (low) intervals. In logging Unit 4 (720–835 m WSF), the resistivity amplitude changes from low to moder-

ate. Likewise, the gamma ray log exhibits the greatest variability compared to the other units. Lithologically, Unit 4 coincides with a thick upper Oligocene–lower Miocene package of chalky sediment with intercalations of dark organic-rich layers. These dark layers are taken as indicators of higher productivity and lower oxygenation during times of deposition.

Although no sonic log or VSP could be run at Site U1468, two high-impedance events identified by distinct lithology changes in the core helped us build a robust velocity model for the time-depth conversion of the seismic horizons. The first impedance event is generated by the top of the densely cemented shallow-water limestone of the Oligocene carbonate platform at 854.7 mbsf (1398 ms TWT) and the overlying wackestone–floatstone; the second is a

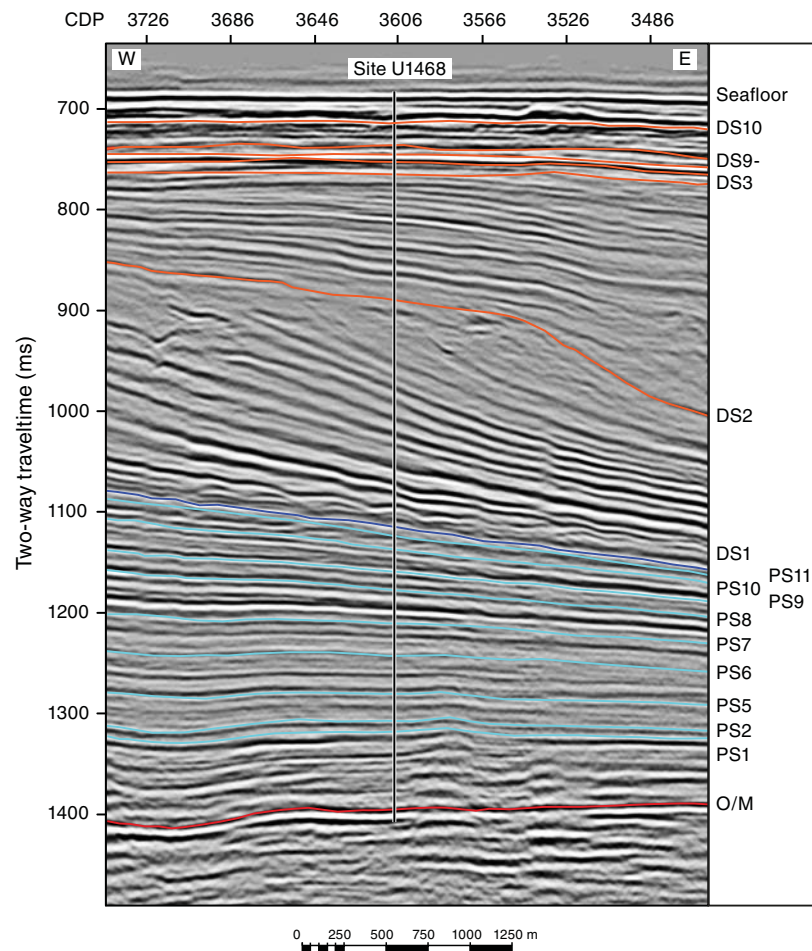
densely cemented grainstone interval with a top surface at 540 mbsf (1198 ms TWT). These two surfaces are used as “check shots” for refining the velocity model.

The penetrated seismic section at Site U1468 displays four main seismic facies (Figure F27). At the bottom are near-horizontal seismic reflections with a distinct high-amplitude reflection that corresponds to the top of the Oligocene shallow-water carbonate platform, which produces the O/M reflection. The O/M reflection was defined by Belopolsky and Droxler (2004a) as the Oligocene/Miocene boundary, but shipboard biostratigraphic analysis of the calcareous nannoplankton and planktonic foraminifers indicates that the Oligocene/Miocene boundary is located further up-section between 769.74 and 779.36 mbsf (i.e., between the O/M horizon and PS1). This interval is composed of a nannofossil chalk package with intercalations of organic-rich layers. Above this chalk package, near-horizontal, low-amplitude reflections occur that are the distal bottomsets of Kardiva platform sequences PS1–PS11 (427.7–724.56 mbsf). These reflections are composed of bioturbated planktonic foraminiferal wackestone to packstone with meter-thick alternations of darker and lighter layers. Sections of

alternating amplitude intensities are likely caused by pulses of sediment deposition, intermittent slow sedimentation, and associated diagenesis (Anselmetti et al., 2000; Malone et al., 2001). The age of these prograding sequences ranges from middle Burdigalian to Langhian or approximately from 21 to 12.7 Ma.

Wavy high-amplitude reflections document the onset of current-dominated sedimentation in the first drift sequences at 434 mbsf. DS1 displays a large mounded geometry with high-amplitude parallel reflections that conjugate basinward. The lower part of DS1 consists of lithified bioclastic packstones to wackestones. DS2 consists of high-amplitude, slightly inclined seismic reflections and is composed of a series of unlithified to partially lithified coarsening-upward packages of large benthic foraminiferal grainstone to rudstone. At the top of DS2, the reflections become nearly horizontal, marking the apex of the drift mound that continues into the base of DS9. At Site U1468, the sequence boundaries of DS3–DS9 merge into two horizontal reflections separated only by approximately 20 m. DS9 and DS10, the uppermost drift sequences, show undulating high-amplitude reflections and a facies of mud-poor bioclastic packstones and grainstones, similar to modern seafloor sediments.

Figure F27. Seismic section of Site U1468 displaying the thick drift succession (DS1–DS10) above the inclined bottomsets of the drowned Kardiva platform (PS1–PS11). A wavy reflection pattern at ~1100 ms TWT marks the onset of the current-dominated sedimentation in the Inner Sea and is the base of DS1. O/M = horizon interpreted by Belopolsky and Droxler (2004b) as the Oligocene/Miocene boundary. DS1 (dark blue) marks the base of the current-controlled sedimentation in the Inner Sea.



Site U1469

Background and objectives

Site U1469 (proposed Site MAL-8A) lies 2.87 km (1.57 nmi) south-southwest of Site U1465, which is the westernmost site of the northern transect in the western part of the Kardiva Channel (Figure F5). It is located at 4°54.41'N, 73°0.48'E, at a water depth of 427 m. The Kardiva Channel formed as a result of the demise of larger carbonate banks during the Miocene (Purdy and Bertram, 1993; Aubert and Droxler, 1996; Belopolsky and Droxler, 2004a, 2004b; Betzler et al., 2009). The northern transect, including Site U1469, is in the approximately 12 km wide northwestern branch of the Kardiva Channel between the Goidhoo and Maalhosmadulu atolls. At present, this passage accommodates seasonally reversing and monsoonal-driven water throughflow. Currents affect the water column down to the sediment surface and trigger erosion at the seafloor and migration of large-scale carbonate sand and mud waves. This depositional regime has persisted since the Miocene, and the hypothesis to test is that the onset of current and partial drowning of the carbonate banks were intimately linked (Betzler et al., 2009; Eberli et al., 2010). Seismic stratigraphy and facies indicate that the onset of this current was a rapid process and that the intensity of the currents varied through time (Lüdmann et al., 2013).

Site U1469 was selected to document and reconstruct the carbonate bank depositional system of the drowned Miocene bank and to link the seismic sequences to facies. The target depth was 700 mbsf, which is the base of PS7, the first sequence after the Kardiva platform went from mostly aggrading growth to progradation.

The specific objectives of Site U1469 were (1) to provide a detailed reconstruction of the predrowning, drowning, and postdrowning evolution of the carbonate bank by linking the seismic stratigraphic record to the sedimentary record; (2) to constrain the timing of this evolution, thus allowing age assignments of unconformities, sedimentary interruptions, sedimentary turnovers, and onset of drift deposition; and (3) to reconstruct and date bank to drift turnover.

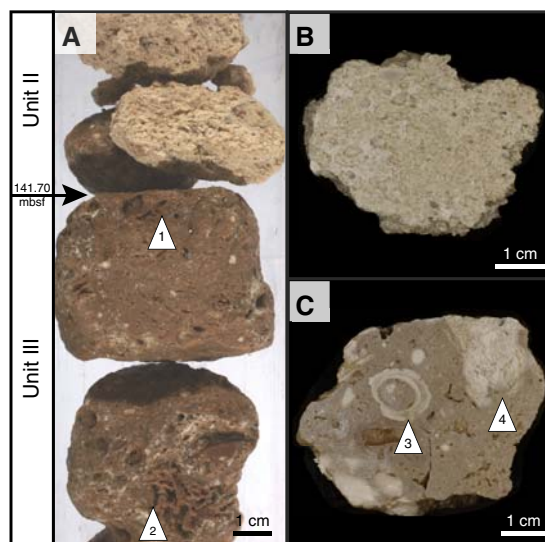
Principal results

The sedimentary succession at Site U1469 was expected to be comparable to that at Site U1465, with a package of loose drift carbonate sands overlying the limestones of the drowned platform. The site was cored with the RCB system because only faulty sleeves for XCB coring were available at the time of drilling. As a result, recovery was very low.

Three lithostratigraphic units are defined at Site U1469 (Figure F3). Unit I (0–93.0 mbsf) represents the youngest hemipelagic deposits, which consist of partly lithified to lithified, gray-brown to pale yellow, coarse-grained, very well sorted grainstone to packstone. Bioclasts are typical open marine pelagic fauna and minor proportions of skeletal benthic fauna that may have originated close to the active atolls and transported by the currents to the Kardiva Channel.

Unit II (93.0–141.7 mbsf) contains coarse-grained grainstone to rudstone with increased amounts of benthic foraminifers and admixtures of corals, bivalves, *Halimeda*, and echinoderm spines. The coarser grain size and the microfaunal assemblage indicate a shallower and higher energy current-dominated environment compared to Unit I. These deposits cover the top of a drowned carbonate platform that makes up Unit III (141.7–153.4 mbsf). The lithologies of Unit III consist of dolomitized coral-rich floatstone with massive and branching coral fragments, rhodoliths, gastropods, and other encrusting organisms interpreted as a shallow-marine reef to forereef setting (Figure F28).

Figure F28. Unit II/III boundary (359-U1469B-4R). A. Transition from white foraminiferal rudstone (Unit II) to grayish brown dolomitized floatstone (dolostone) (Unit III). 1 = boring, 2 = coral fragment. B. Bioclastic grainstone with benthic foraminifers (Unit II). C. Dolomitized floatstone (Unit III). 3 = encrusting red algae, 4 = coral fragment.

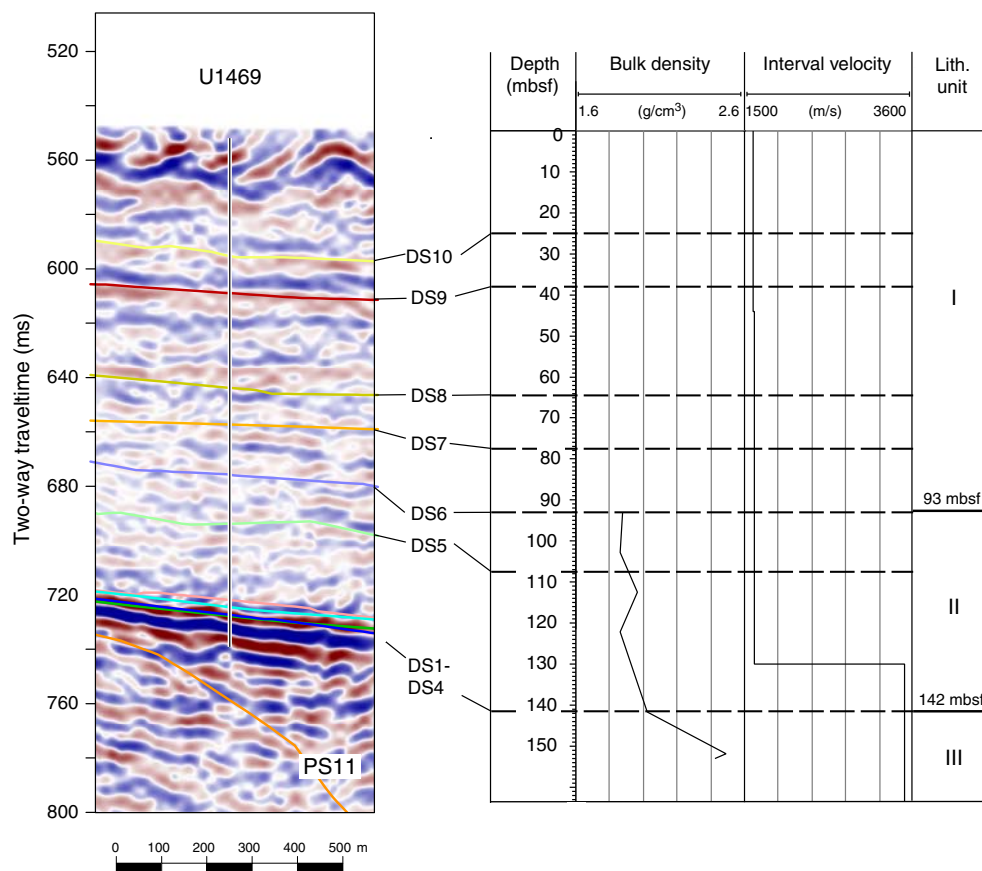


Because of poor recovery, no continuous record of core catchers could be obtained. As a result, the biostratigraphic age model for this site is limited, but both the planktonic foraminifers and the calcareous nannofossils indicate a Quaternary to early Pliocene age for sediments above the drowned platform. Planktonic foraminifer biostratigraphy identified two Pleistocene biohorizons, the LOs of *Globigerinoides fistulosus* (1.88 Ma) and *Globorotalia limbata* (2.39 Ma), which were found at 44.57 and 63.96 mbsf, respectively. The Pliocene LOs of *Dentoglobigerina altispira* (3.47 Ma) and *Globorotalia margaritae* were found at 63.96 and 73.7 mbsf, respectively. The occurrence of nannofossils is sparse and poorly preserved. Thus, no assemblages are unambiguously datable. However, the presence of small *Gephyrocapsa* specimens in the upper part of the sequence (25–93 mbsf) indicates that these samples are Quaternary to middle Pliocene in age (Zones NN21 to NN14). Similarly, the consistent presence of *Sphenolithus* specimens in the lower part of the site (73.6–122.1 mbsf) suggests that this part of the sequence is middle Pliocene or older (Zone NN15 or older), although they could be reworked. No Miocene marker species were seen. The drowned platform does not contain any age-diagnostic benthic foraminifers, but seismic stratigraphic evidence places a middle Miocene age at the drowning surface.

Seven sediment samples above the platform yielded carbonate contents between 94.95 and 97.95 wt%, and their total organic carbon is between 0.04 and 0.15 wt%. The mineralogy of the sediment consists of aragonite, HMC, LMC, and dolomite. HMC is present only to 25 mbsf and reaches a maximum of 8.9%. Aragonite occurs at concentrations between 10.7% and 49.0% from the surface to 73.6 mbsf. Below this depth, most of the aragonite and all of the HMC neomorphosed to LMC. Dolomite is present with a low abundance of <3.3% above 93 mbsf. Below 93 mbsf, dolomite increases to concentrations between 4.4% and 30.9% and the concentration of aragonite decreases. The platform carbonates at 153.22 mbsf are completely dolomitized.

One paleomagnetic reversal is recognized at 153.8 mbsf and is normal below. In addition, a possible short reversal occurs at 153.9 mbsf.

Figure F29. Correlation of seismic and core data, Site U1469. Seismic Line 32 (SO236) is shown with the platform and drift sequences. The few recovered rocks yielded some bulk density information. Interval velocity profile is taken from Site U1465.



Physical properties fall into two groups that correspond to the Pliocene–Pleistocene drift sediments (physical properties Unit 1) and the carbonate platform succession (physical properties Unit 2). The slightly lithified grainstone to rudstone facies of the drift sediment displays low NGR that increases downhole. As in the drift sediments of the other sites, bulk density is low (1.5–2.0 g/cm³), porosity is very high, ranging from 42% to 52%, and *P*-wave velocity reaches 2562 m/s. The dramatic facies change to platform carbonates at 141.7 mbsf is reflected in the physical properties. The dolomitized limestone has high NGR values. Bulk density averages 2.5 g/cm³, whereas grain density is 2.84 g/cm³, confirming the complete dolomitization of this interval. Porosity is between 15.4% and 22.8%. Despite relatively high porosity, velocities are over 5000 m/s. This can be explained by the dominance of the moldic pore types that produce a rock with a stiff framework.

The time–depth conversion for correlating the seismic data to the lithology relied on the velocity model from Site U1465, which has a similar lithology. Similar to Site U1465, Site U1469 is at the margin of the drowned Kardiva platform and overlain by drift deposits (Figure F29). At this location, however, the sequence stratigraphic interpretation indicates a younger age for the top of the Kardiva platform. Additionally, the drift sequences overlying DS4 are more complete. The seismic facies of the drowned Kardiva platform displays a series of prograding clinofolds with slightly basinward inclined topsets and steep foresets that flatten out basinward. The overlying drift deposits are horizontal, semicontinuous, medium-amplitude reflections of DS4–DS10 and are interpreted to be

late Miocene to recent in age. However, no age-diagnostic fossils were found in the portion directly overlying the drowned platform. The drowned platform top is part of PS11, which was interpreted to be middle Miocene in age. Shore-based radiometric dating will be needed to assess the exact age.

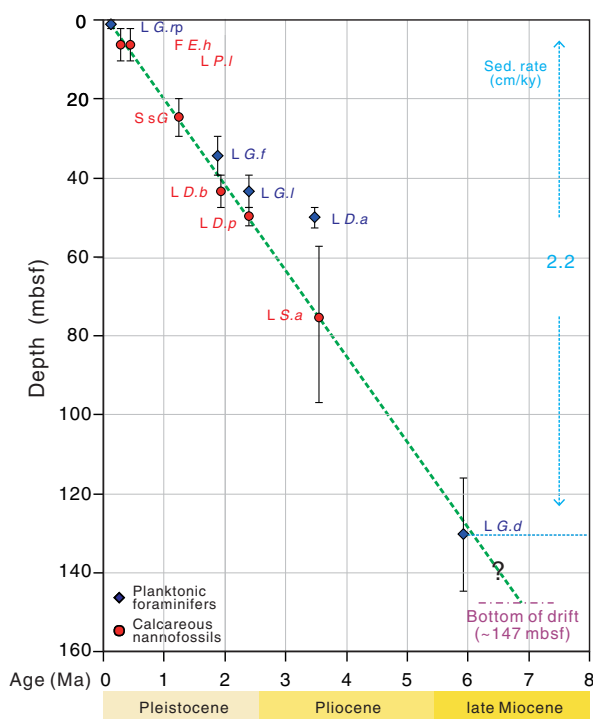
Site U1470

Background and objectives

The western Kardiva Channel that connects the open Indian Ocean with the Inner Sea of the Maldives is divided into northern and southern branches by the Goidhoo atoll. The second transect of sites drilled during Expedition 359 is located in this southern branch of the Kardiva Channel. Site U1470 is the westernmost site of this southern transect (Figure F5) and has a geographical position of 4°45.9823'N, 72°59.0267'E, and a water depth of 399.7 m.

The site was positioned where seismic data indicated that a carbonate platform existed during the early stages of drift deposition. This seismic relationship implied that at this location the platform drowning is younger than in the northern Kardiva Channel. The main goal at Site U1470 was therefore to recover the drift to platform succession, which contains a platform that drowned at a later stage than the platforms in the northern transect. The specific objectives were (1) to provide a detailed reconstruction of the predrowning, drowning, and postdrowning evolution of the carbonate bank by linking the seismic stratigraphic record to the sedimentary record; (2) to constrain the timing of this platform drowning and the burial by drift sediments; and (3) to reconstruct

Figure F30. Age-depth plot, Site U1470. L = last occurrence, F = first occurrence. *G.r.p* = *Globigerinoides ruber* pink, *E.h* = *Emiliana huxleyi*, *P.l* = *Pseudemiliana lacunosa*, *S.s.g* = Start small *Gephyrocapsa* event, *G.f* = *Globigerinoides fistulosus*, *D.b* = *Discoaster brouweri*, *G.l* = *Globorotalia limbata*, *D.p* = *Discoaster pentaradiatus*, *D.a* = *Dentoglobigerina altispira*, *S.a* = *Sphenolithus abies*, *G.d* = *Globoquadrina dehiscens*.



the neritic carbonate factory of a bank growing in the current-dominated depositional system.

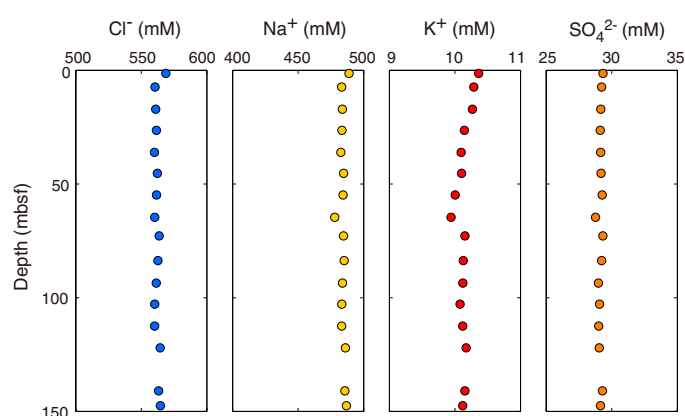
Principal results

Site U1470 penetrated 147.9 m of carbonate sand and 186.2 m of limestone from the underlying carbonate platform (Figure F3). The uppermost 59.1 m (lithostratigraphic Unit I) of the sheeted drift deposits was unlithified coarse-grained grainstone to packstone with abundant planktonic foraminifers but also benthic foraminifers, ostracods, pteropods, echinoderm spines, bryozoan fragments, and bivalves, as well as yellow-red-stained lithic grains and red algae fragments. In lithostratigraphic Unit II (59.1–147.8 mbsf), the grainstones become more lithified and the composition changes to a diverse assemblage of bioclasts.

Three lithostratigraphic units were identified in the platform succession. Unit III (147.9–188.4 mbsf) comprises coral-rich floatstone to boundstone, documenting a shallow-water reefal environment at the top of the drowned platform. Unit IV (198–207.7 mbsf) is bioclast-rich grainstone to rudstone that, with its composition of large benthic foraminifers, red algae, green algae (*Halimeda*), and coral fragments, resembles a reef-apron facies. Unit V (207.7–334.11 mbsf) is a reef facies with interbedded grayish brown coral-rich boundstone and red algae floatstone. Coral fragments include massive, platy, and branching forms. Rhodoliths are present in different sizes up to 4 cm long with branching irregular shapes.

Micropaleontological analysis (Figure F30) of core samples from the drift package above the platform carbonates allowed us to define a sequence of biostratigraphic events and a well-constrained age model for the upper part of the sedimentary succession that spans

Figure F31. IW Cl^- , Na^+ , K^+ , and SO_4^{2-} concentrations, Hole U1470A. Concentrations of major anions and cations display near constant and close to seawater values, although changes in carbonate mineralogy occur in the same interval. This pattern was observed at several other sites during Expedition 359 and might be the result of massive advection that dilutes the signature of diagenesis in the pore water of highly porous drift sediment.



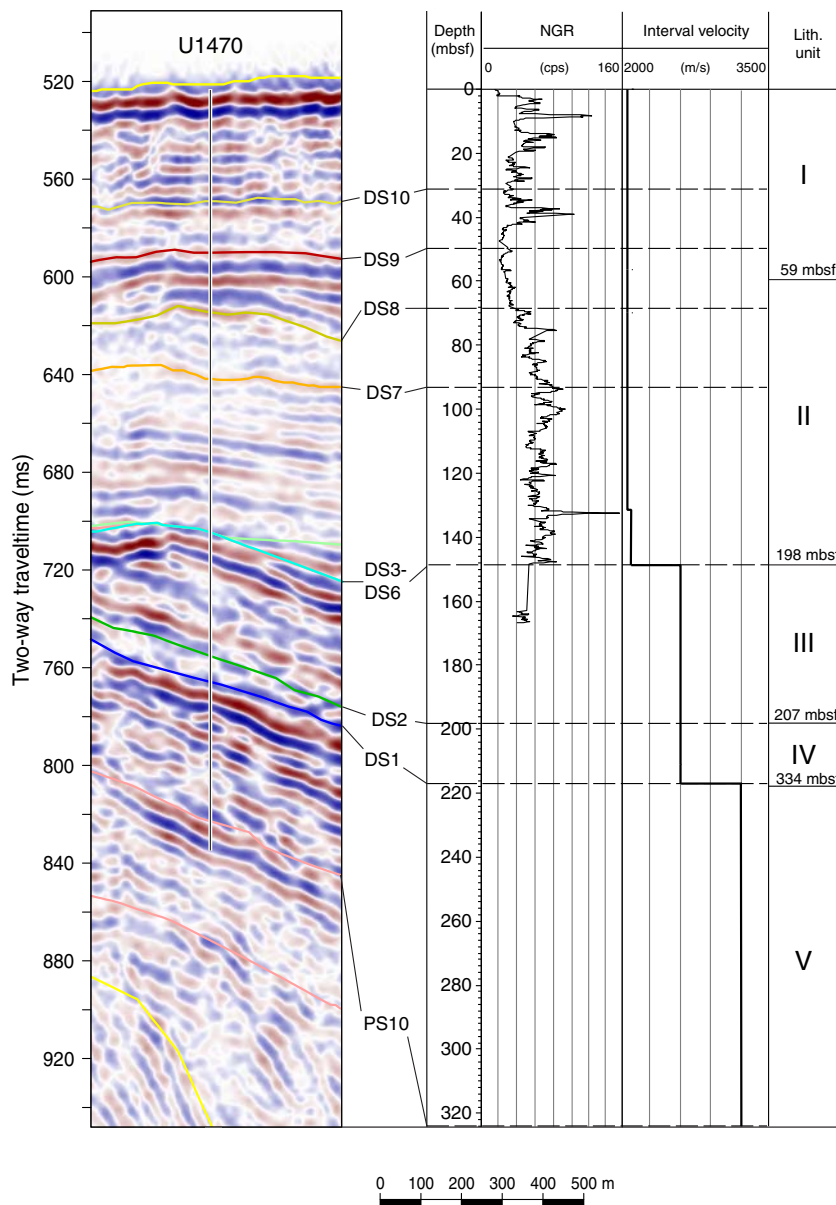
from the Quaternary to the lower Pliocene. As at other sites, however, throughout this interval the planktonic foraminifers consistently indicate older ages and lower sedimentation rates than the calcareous nannofossils. For the lower part of the cored interval, lower Pliocene and possibly uppermost Miocene, only a single planktonic foraminiferal event was identified. This suggests that the sedimentation rate remained constant throughout the Pliocene at ~2.2 cm/ky and that the base of the drift sequence overlying the drowned platform top is older than 5.92 Ma.

The concentrations of major anions and cations determined from IW chemistry display near constant and close to seawater values through the uppermost 150 m of the unlithified drift sediments. This lack of gradient and thus indication of diagenetic alteration is in contrast to the changes in carbonate mineralogy across the same interval that document the disappearance of HMC and formation of small amounts of dolomite (Figure F31). This pattern was observed at several other sites during Expedition 359 and might be the result of massive advection that dilutes the signature of diagenesis in the pore water of highly porous drift sediment. The drowned platform cored at Site U1470 is mostly limestone with only a short interval with 20% dolomite and preserved aragonite between 200 and 250 mbsf. In the platform strata recovered at Sites U1469 and U1465, the drowned platform is considerably more dolomitized.

The paleomagnetic analysis was severely hampered by a persistent contamination that typically affected the first two sections of each core (this problem was already observed at the other sites) and a novel artifact that mostly affected measurements below 60 mbsf in Hole U1470A. Starting from Core 359-U1470A-8H, the measured paleomagnetic directions of the “uncontaminated” portion of each core show a constant direction toward east with a subhorizontal inclination (~090/00) independent of the actual core orientation. Given all the uncertainties associated with these measurements, we did not attempt to interpret these results as a record of geomagnetic polarity changes.

The sedimentary succession from Site U1470 is divided into three physical properties units based on the changes observed in NGR, *P*-wave velocity, bulk density, and porosity measurements. Physical properties Units 1 and 2 (0–148 mbsf) comprise upper Miocene to recent drift sediments. The entire package has very high porosity, although in Unit 1 porosity decreases from 80% to 60%

Figure F32. Correlation of seismic and core data, Site U1470. Seismic Line 32 (SO236) is shown with the platform and drift sequences. Interval velocity is used for the time-depth conversion.



with a more gradual decrease ranging from 60% to 40% in physical properties Unit 2. Sonic velocity is low (average = 1725 m/s) and increases slightly to the bottom of Unit 2. NGR fluctuates with high frequency throughout these two units but has a low at the unit boundary. Physical properties Unit 3 (148–334.1 mbsf) consists of samples from the carbonate platform succession with high velocity and density values and a concomitant decrease in porosity. Velocity varies widely from 2000 to 5000 m/s.

Seismically, the drift sequences overlying the drowned platform are mostly subparallel, semicontinuous reflections, mainly of medium amplitude. DS10 and DS9 correspond to drift deposits of unlithified planktonic foraminifer-rich grainstone. This package is followed by the partly lithified bioclastic grain- to packstone of lithostratigraphic Unit II, which comprises DS3–DS8. The bounding unconformity of DS3 corresponds to the top of the shallow-water platform limestone (lithostratigraphic Unit III). The top of the

coral-rich boundstone and floatstone in lithostratigraphic Unit V is the reflector for DS1 (Figure F32). This platform package thins out and DS3 and DS2 almost merge 400 m to the west. DS1 and DS2 at this locality therefore bear a platform succession that postdates the drowning event recognized at Sites U1465 and U1469. The DS2 bank is characterized by an elevated top and shows basinward-dipping reflections in its eastern part. To the west, these reflections abut the basal sequence boundary of DS3, which can be explained by two processes. This stratal pattern could show a late-stage predrowning reef package, or it might reflect erosion of the reef-related strata.

Site U1471

Background and objectives

Site U1471 is the eastern end of the southern transect at 4°45.9828'N, 073°08.1146'E, in a water depth of 419.3 m in the In-

ner Sea (Figure F5). The site is positioned on the distal portion of the prograding drift where it thins and is overlain by the sheeted drift deposits. The target depth is in the distal bottomsets of the sea level–controlled platform sequences underneath the drift, estimated to be at about 950 mbsf (Figure F8). At this location, all sequence boundaries are conformable; therefore, cores from this site were expected to provide a continuous and expanded record of current evolution from the middle Miocene throughout the Pleistocene.

The specific objectives for Site U1471 were (1) to constrain the age of onset of current-dominated sedimentation; (2) to analyze the cyclostratigraphy of drift deposits, therefore providing reconstructions of changes in the current regime and monsoon cyclicality; and (3) to constrain the timing of sequence boundaries within the drift and the youngest platform sequence.

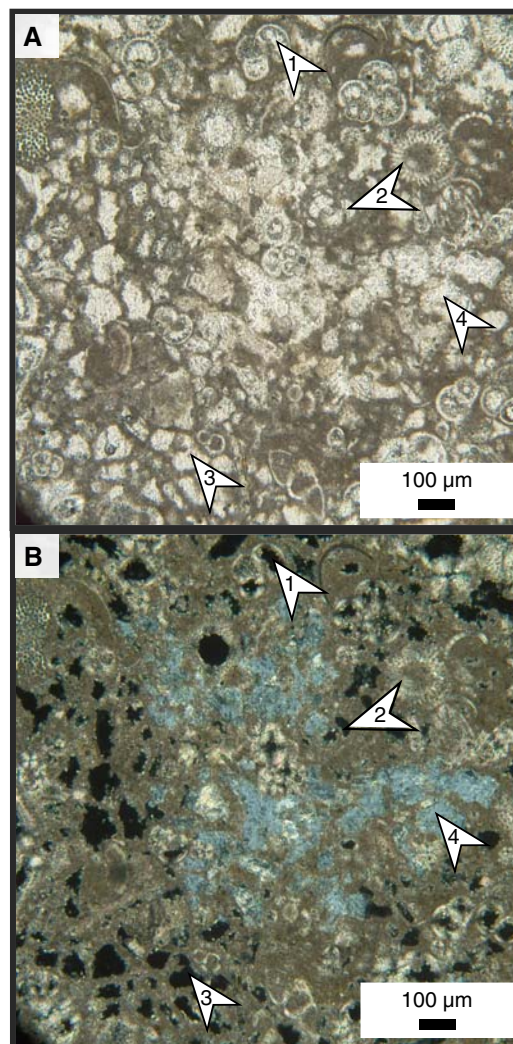
Principal results

An 889 m thick succession of drift deposits above 110.9 m thick distal platform bottomsets was retrieved at Site U1471. Seven lithostratigraphic units are distinguished in the drift deposits that reflect the degree of current-controlled winnowing and diagenetic overprint (Figure F3). Unit VIII comprises the periplatform deposits in the distal bottomsets. Units I–III (0–180.1 mbsf) consist of planktonic foraminifer–rich packstone to wackestone that is heavily bioturbated, often producing a mottled appearance. All three units contain benthic foraminifers, echinoderm spines, pteropods, sponge spicules, calcareous nannofossils, and mollusk fragments in addition to abundant planktonic foraminifers. The degree of lithification was used to distinguish un lithified Unit I from partly lithified Unit II, and the predominance of the wackestone texture was taken as the criteria to separate Unit III. All three units contain alternations of intervals with darker and lighter colors. These alternations range from ~1 to 10 m, and the darker portion of the alternation is generally much thinner (~20% of the total). The dark intervals comprise higher amounts of organic material and tunicates but fewer benthic foraminifers compared to the lighter intervals.

Units IV (180.1–254.6 mbsf) and V (254.6–588.2 mbsf) have similar textures and consist predominantly of planktonic foraminifer–rich packstone. These units differ in the amount of lithification rather than composition, with alternating lithified and un lithified layers in Unit IV. Unit V contains densely cemented layers and layers with moldic porosity. Unit IV has some wackestone intercalations that are generally less lithified than the packstone. In both units, overgrowth of bioclasts was prevalent. Several intervals in Unit V exhibit visible porosity, including intraparticle, moldic, and vuggy porosity. At times, celestine is present, forming large crystals spanning adjacent pores (Figure F33).

Unit VI was defined by the occurrence of alternations of very fine to medium-grained dark brownish packstone and dark brownish gray to light gray wackestone/packstone. In addition to planktonic foraminifers, sponge spicules, radiolarians, and calcareous nannofossils were identified, as well as rare dolomite crystals. Packstone intervals are thinner than those comprising wackestone and are less bioturbated than wackestone intervals; individual burrows are discernable, and lamination-like structures are present. The burrows are in some cases completely flattened, and some of the discontinuous lamination-like structures may be highly compacted burrows, possibly with organic matter. *Planolites*, *Chondrites*, *Palaeophycus*, *Phycosiphon*, *Thalassinoides*, *Teichichnus*, and *Zoophycos* ichnofossils were identified, in that order of abundance.

Figure F33. Components, porosity, and cementation of packstone in Unit V (359-U1471A-38X-1). Degraded foraminifers punctuated by (1) intraparticle, (2) moldic, and (3) interconnected vuggy porosity. Pore space is partially filled by (4) celestine (blue color; arrow). A. PPL. B. XPL.

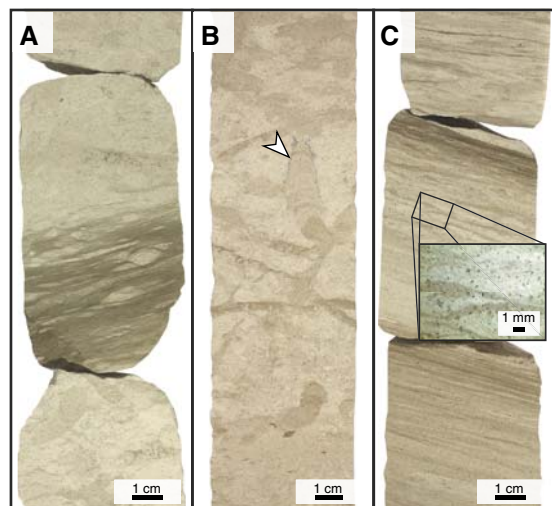


Fractures in incompletely cemented beds occur as both open and cemented fractures.

Unit VII contains thin, loosely cemented grainstone layers in background sediment of fine-grained foraminifer-rich packstone. The light brownish gray to light gray coarse-grained bioclastic-rich grainstone is between 2 and 78 cm thick (average = 14.0 cm). The layers often (but not always) have sharp lower boundaries and a more gradational top. Grain size does not vary much within the grainstone layers. These layers were interpreted as reflecting high-energy current events within the first drift sequence.

In the distal bottomsets of the prograding clinofolds of Unit VIII, the facies changes considerably from very fine to fine-grained, white to light gray, foraminifer-rich packstone to wackestone and from very fine grained and finer dark gray wackestone to mudstone. Calcareous nannofossils are abundant in both end-members; planktonic foraminifers are abundant in the lighter packstone to wackestone and rare in the dark wackestone to mudstone. Benthic foraminifers and glauconite are present only in the lighter packstone to wackestone. In the lighter intervals, bioturbation is com-

Figure F34. Sedimentary features in Unit VIII. A. Alternations between white and dark gray layers (359-U1471E-35R-3). B. Glauconitic rims around burrows (arrow) (34R-6). C. Fine pseudo-lamination structure (36R-2). Insert shows discontinuous internal structure, possibly tapered and flattened burrows.



mon with ichnofossils, including *Planolites*, *Thalassinoides*, *Zoophycos*, and *Chondrites* (Figure F34).

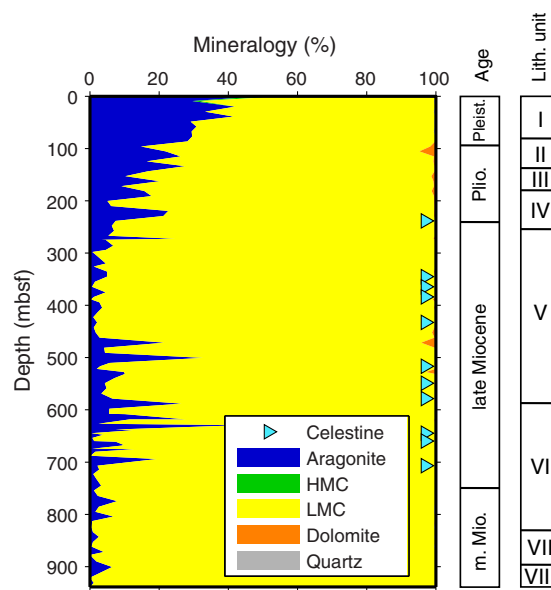
Biostratigraphic and paleoenvironmental analyses in Holes U1471A, U1471C, and U1471E provide a robust age model at Site U1471. Pleistocene and late Pliocene sediments extend from the seafloor to ~150 mbsf and are defined by a succession of well-constrained events and reasonably good agreement of the data. The implied sedimentation rate is 4.0 cm/ky. However, there is a consistent offset between the ages inferred from calcareous nannofossil events and those from planktonic foraminifers, with the planktonic foraminifers suggesting ages about 0.5 My older than the calcareous nannofossils. This pattern was also seen in this interval at Sites U1465–U1467, so possibly the age calibrations of these events may need revision, at least for this area.

In the underlying bottomsets, preservation of planktonic foraminifers is generally moderate to very poor. Benthic foraminifers are moderately preserved throughout this interval, with preservation decreasing downhole. Nannofossil preservation is poor to moderate throughout most of the core. In the lower part of Hole U1471E (Cores 37R–44R), nannofossils are generally more abundant and better preserved. The planktonic foraminiferal and nannofossil events recognized in this lower Pliocene to mid-Miocene section reasonably agree with each other. They provide an inferred sedimentation rate of 8.0 cm/ky.

The concentrations of major anions and cations in IW of the upper 40 mbsf exhibit negligible changes. Below this interval, pore water profiles of many elements start to vary, indicating numerous diagenetic processes occurring in the sediment column. The inflection points of these profiles, however, do not coincide with boundaries between lithostratigraphic units.

A decrease of sulfate coincided well with an increase in alkalinity, indicating that bacterial sulfate reduction is occurring in the sediment column. However, a greater increase in alkalinity was expected from the ~4 mM decrease in sulfate than was observed; the difference is explained by the authigenic precipitation of calcite. The decrease in Mg^{2+} and concurrent increase in Ca^{2+} reflects dolomitization by replacement of calcium carbonate. However, only a

Figure F35. Relative concentrations of aragonite, HMC, LMC, dolomite, and quartz measured using XRD, Site U1471.



minor amount of dolomite was found at this site, with the dolomite peak at 105.55 mbsf occurring close to the maximum decrease in Mg^{2+} concentrations. A rapid increase in the Sr^{2+}/Ca^{2+} ratios of the pore water occurs below 40 mbsf, documenting the neomorphism of aragonite sediments to LMC, which is also evident in the changes in carbonate mineralogy based on the XRD data (Figure F35). The large increase in Sr^{2+} caused the pore fluids to attain saturation with respect to celestine ($SrSO_4$). The presence of celestine and high sedimentary Sr/Ca ratios extends to approximately 700 mbsf. Changes in the Mn content of the pore waters and sediments were related to the redox state. The higher Pliocene–Pleistocene Mn/Ca and Fe/Ca ratios may reflect a more reducing environment during this time interval relative to the late Miocene. The small increase in Mn/Ca and Fe/Ca in the middle Miocene may be coincident with the development of the Oxygen Minimum Zone as proposed by Dickens and Owen (1994).

A cyclic pattern in carbonate content is visible when the data are smoothed with a five-point moving average, with alternations of ~5 wt% between higher and lower values. The upper 300 mbsf has a period of ~40 m with seven or eight maxima within this depth interval. Where recovery was poor, from 300 to 400 mbsf, the smoothing was not effective, but cycles with an amplitude of ~5 wt% carbonate were again apparent between 400 and 1000 mbsf. The apparent cycles in carbonate content may be related to changes in climate or currents, which influenced sediment supply and probably carbonate dissolution at Site U1471.

For establishing a magnetostratigraphy at Site U1471, the core-orienting device was used in the upper 19 cores drilled in Hole U1471C and in Cores 359-U1471D-6H and 7H. The magnetostratigraphy is based on the interpretation of the declinations in the oriented APC cores that show relatively consistent directions within each core, with most of the reversals occurring within a single core. The Brunhes/Matuyama boundary was tentatively placed between Cores 359-U1471C-4H and 359-U1471D-6H (36–39 mbsf) based on the short reversal found in Core 359-U1471D-5H, which was interpreted as the Jaramillo Event. Additional reversals were identi-

fied at 79, 84, 112, 152, 169, and 172 mbsf (Cores 359-U1471C-9H, 10H, 12H, 16H, and 19H).

Analysis of physical properties allowed us to divide the sedimentary formation into six units primarily based on porosity and NGR measurements and not necessarily following lithostratigraphic unit boundaries. In physical properties Unit 1 (0–68 mbsf), sediments have high porosity values of 60%–75% decreasing downhole within the unit. Porosity, however, increases again downhole in physical properties Unit 2 (68–138 mbsf) to reach 75%. A similar reversal of the porosity trend occurs in the lower part of the succession in physical properties Unit 6 (700–1003 mbsf), where porosity values reach around 50% and are on average higher than in physical properties Unit 5 (320–700 mbsf). NGR counts reach values higher than 80 counts/s in physical properties Unit 4 (180–320 mbsf) and are the highest NGR values measured on Expedition 359 cores.

Three logging runs were conducted at Site U1471, but only the triple combo tool string reached the bottom of the hole. The VSI tool string encountered an impassable obstruction at ~615 m WSF, and the FMS-sonic tool string did the same at 454 m WSF. The triple combo tool string produced good quality data, except in three intervals where the borehole diameter was too large. Gamma ray values are dominated by uranium, as at other sites. The porosity log confirmed the high porosities measured in the laboratory and the unusual high porosities of the drift deposits. Resistivity and magnetic susceptibility display similar trends and increase slightly downhole between 50 and 400 m WSF. They decline from there to the bottom of the hole but have a small but abrupt drop at the bottom of the drift. In the short interval velocity was measured, it displays a gradual increase with depth to 400 m WSF with a few higher peaks. In the deepest 40 m of the log data (400–440 m WSF), velocity fluctuates dramatically and reaches as high as 3.5 km/s. These fluctuations match the alternating lithified and unlithified lithologies observed in the cores. Four formation temperature measurements documented a low geothermal gradient of 15.3°C/km.

Determining the relative positions of core gaps among the various holes at Site U1471 during coring was accomplished using gamma ray attenuation (GRA) density data collected at 5 cm resolution on the Whole-Round Multisensor Logger (WRMSL). NGR was also used to evaluate sedimentary completeness for Holes U1471A, U1471C, and U1471D. High-resolution compositing was based on the 2.5 cm interval color reflectance parameter L^* for all but one interval where L^* lacked distinct patterns. The composite depth scale and splice at Site U1471 are constructed from 0.0 to 195.71 m CCSF-D; deeper cores from Hole U1471A are appended with a constant affine value.

The upper 30 m of the L^* records from Sites U1467 and U1471 were compared to assess Late Pleistocene sections at each site. This interval was correlated to 0–800 ka at Site U1467. Based on the L^* records, the latest Pleistocene is slightly more expanded at Site U1467 than Site U1471 over the interval correlated to marine isotope Stages (MIS) 1–11. Below this level, the reflectivity L^* highs are more expanded at Site U1471 than Site U1467. The change in relative thickness of the reflectivity highs between Site U1467 and U1471 sedimentation may indicate subtle changes in the location of current-controlled sedimentation at ~450 ka.

Seismic stratigraphy and core data were correlated using three stations of the check shot survey with the VSI tool string in the upper part of the hole. To anchor our velocity model in the interval below 604.6 mbsf, where hole collapse prevented further lowering of the tool, we used the boundary between lithostratigraphic Units VII and VIII (Core 359-U1471E-33R), which marks the change from

drift to platform sequences at 898 mbsf, as a tie point. The three oldest drift sequences (DS1–DS3) at Site U1471 show a pronounced clinof orm prograding reflection pattern. DS5–DS10 are classified as elongated mounded separate drifts. Site U1471 penetrated the bottomsets of the prograding drift bodies, calibrating the seismic facies with the depositional facies. For example, high-amplitude reflections, especially in DS3, are related to strong impedance contrasts produced by the alternation of partly lithified and lithified beds. In DS3 and DS4, small-scale wavy reflections are interpreted as cyclic steps or bottom current–related features.

Correlation of the seismic sequences and the biostratigraphic age model shows that DS9 encompasses the Pleistocene. The pronounced change in lithology between lithostratigraphic Units IV and V at 254.6 mbsf correlates with the base of DS4 (261.5 mbsf) and roughly coincides with the boundary between the Pliocene and Miocene. The bottom of the drift that is the base of DS1 at 898 mbsf lithologically expresses the last occurrence of grainstone layers at 898 mbsf in the upper middle Miocene.

Site U1472

Background and objectives

Site U1472 is in the middle of the southern transect at 4°46.2653'N, 073°04.0111'E, at a water depth of 379.34 m (Figure F5). The site is located well within the middle part of the west to east prograding drift fan. The target for coring at this site was the lower sequence boundary of DS1, but it was not reached because of time constraints at the end of the expedition. Coring penetrated to 251.9 mbsf and recovered 233.75 m (93%), providing a valuable data set for understanding drift deposition in the Inner Sea and the contourite fan depositional system. The specific objectives at this site were (1) to constrain the ages of the drift depositional sequences; (2) to analyze the cyclostratigraphy of drift deposits, therefore providing reconstructions of changes in the current regime and monsoon cyclicity; and (3) to retrieve the lithology of the wavy seismic facies to confirm their current-controlled deposition.

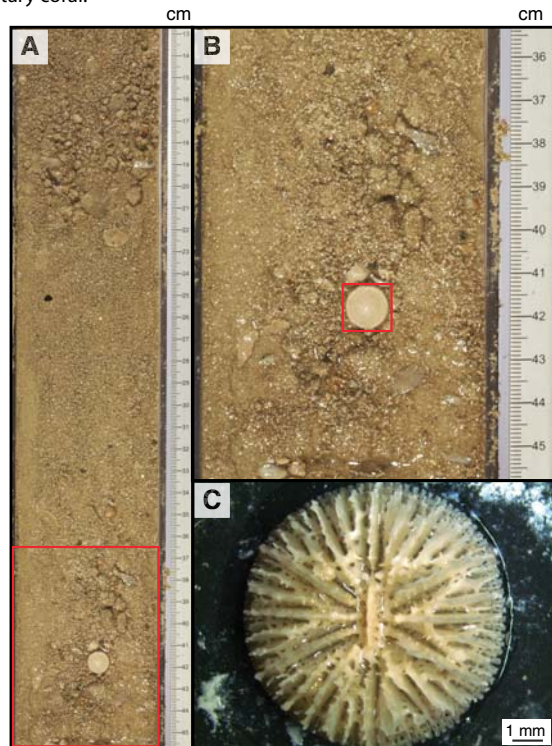
Principal results

The succession at Site U1472 is divided into four lithostratigraphic units (Figure F3). Unit I (0–52.70 mbsf) consists of unlithified packstone and grainstone texture and mud-lean fine to medium sand. Deposits contain abundant fairly well preserved planktonic foraminifers, pteropods, otoliths, echinoid fragments, and shell fragments. Layers of floatstone contain large bioclasts such as pteropods and solitary corals (Figure F36). Light gray to brownish gray sediment was interpreted to reflect the presence of organic matter and also of iron in reduced form. This sediment provides evidence for suboxic conditions at the seafloor, as does the NGR measured on the cores. Varying gray-brown color changes associated with a cyclic pattern of L^* color reflectance and NGR likely indicate that these conditions fluctuated through time.

Unit I has grainstone to packstone textures, lithostratigraphic Unit II (52.70–195.20 mbsf) consists of packstone to wackestone but has a similar composition. NGR values in Unit II are distinctly lower than in Unit I, and the top of Unit II contains large bioclasts and shells, suggesting a phase of intensified bottom current.

The transition from packstone to grainstone texture and the grain size change from predominantly medium- to coarse-grained grainstone-packstone define the top of Unit III. Unit III is characterized by the appearance of large benthic foraminiferal assemblages typical of neritic environments. Foraminiferal shells have extensive overgrowths, masking their original shape. The textural,

Figure F36. Components of Unit I. A. Unlithified floatstone with grainstone matrix (359-U1472A-4H-1, 3–46 cm). Red box = area in B. B. Unlithified floatstone with large components such as a solitary coral (detail shown in C), intraclasts, echinoid fragments, and mollusk fragments (4H-1, 35.5–45.5 cm). C. Solitary coral.



grain size, and biota assemblage changes collectively imply that this unit represents a shallowing-upward succession.

Unit IV (224.22–249.24 mbsf) is marked by a change toward coarse-grained grainstone texture. The bioclast assemblage is composed of corals, red algae, large benthic foraminifers, and bivalves. Texture, grain size, and inclined layers indicate that these sediments were deposited under high-energy conditions that existed on the top of the drift fan drift sequence.

Calcareous microfossils are present throughout the sequence, showing good preservation in the upper 100 m and poor to very poor preservation below. The calcareous nannofossil biostratigraphy suggests a late Miocene age for the bottom of the sequence. A useful sequence of biostratigraphic events through the Quaternary and early Pliocene provides a fairly clear age model that indicates a sedimentation rate of 2.6 cm/ky throughout the succession. As observed at other Expedition 359 sites, planktonic foraminifers in this interval consistently indicate older ages and therefore lower sedimentation rates than those based on calcareous nannofossils.

IW analysis indicates that the slight increase in chloride in pore waters at Site U1472 is higher than the increase observed at Site U1471 but not as strong as that at Sites U1466 or U1468. This may be a relict signal of Last Glacial Maximum seawater that has not yet diffused. Negligible rates of bacterial sulfate reduction relative to advection of seawater at Site U1472 are indicated by the constant alkalinity concentrations with depth. Neomorphism of aragonite to LMC does not appear to occur with the same intensity as at other Expedition 359 sites. The high abundance of aragonite even at 200 mbsf is unique to this site and may be related to the general lack of modern, active diagenesis inferred from constant pore fluid pro-

files. The constant alkalinity at Site U1472 also implies that the small amounts of dolomite present in the sediments are the result of previous episodes of alteration and are not actively forming in the modern sediment column. Carbonate diagenesis and dolomitization must have occurred in previous time intervals but do not seem to have resulted in aragonite neomorphism to LMC.

Measurements of the magnetic sediment properties exhibit early vertical and negative inclinations in the uppermost 30 mbsf of Hole U1472A that could be interpreted as a coring disturbance in these soft and fluid-rich sediments. The rest of the inclination record, although it shows generally shallower inclination, still has a rather erratic behavior that was not easily interpretable as a sequence of reversals.

Because of time constraints at the end of the expedition, only a reduced suite of physical property measurements was performed on Site U1472 cores (primarily whole-round and split-core track measurements). Four physical properties units are observed and correlate well with the lithostratigraphic units. Physical properties Units 1 and 2 have high NGR values in their lower parts and decreasing values toward the top. Physical properties Units 2–4 generally show lower NGR values with little variation but some isolated peaks of higher values. Sediment bulk density at Site U1472 increases continuously downhole, whereas there is an inversion of the *P*-wave velocities below 185 mbsf. As at other sites, porosity is very high at the top (>70%) and decreases to ~50% at 200 mbsf.

For a time to depth conversion, the check shot information from Site U1470 was used because the sediments had similar characteristics at both sites. DS7–DS10 are sheeted; they are imaged by well-stratified continuous reflections of medium to low amplitude. The subhorizontal reflections of the topsets of DS4–DS6 are discontinuous to wavy at Site U1472, but the reflections become more continuous in a distal direction to the east. Whereas DS5 and DS6 are sheet-like, DS3 and DS4 have a divergent pattern and thicken basinward. The calibration of these seismic facies was one of the objectives for Site U1472.

Lithostratigraphic Unit I corresponds to Pleistocene DS10 and DS9. DS8–DS5 are dominated by packstones, which become increasingly lithified with depth. The transition from lithostratigraphic Units III to IV at 224 mbsf corresponds with the DS3/DS4 boundary and is accompanied by a significant increase in benthic foraminifers and by more diverse skeletal components. Both DS3 and DS4 show a characteristic chaotic reflection pattern of high amplitude that correlates well to the abundance of coarse material in lithostratigraphic Units III and IV and layers with downcutting erosion. Both features indicate a high-energy depositional regime within this drift sequence.

Preliminary scientific assessment

Eight sites were drilled along two transects in the Kardiva Channel in the Inner Sea of the Maldives during Expedition 359. The recovered cores retrieved material to achieve all of the objectives set for the expedition. Beyond the acquisition of these data, coring also revealed a series of unexpected discoveries.

Drilling the carbonate platforms and drifts in the Maldives aimed to recover the marine tropical record of the Neogene sea level changes and the onset of the monsoon-related current system in the Indian Ocean. The recovered cores and log data elucidate both aspects with great detail. The most arresting accomplishment is the documentation of how the sea level-controlled carbonate

platform system thrived during the mid-Miocene Climate Optimum and abruptly transitioned into a current-dominated system in the late middle Miocene. This transition is thought to be linked to the onset of an early intensification of the Indian monsoon and the coeval demise of parts of the Maldivian platform. In addition to accomplishing all of the primary objectives, four major discoveries were made, and all are major contributions to the fields of paleoceanography, sedimentology, biostratigraphy, and geochemistry. How these objectives and the additional discoveries were achieved is outlined below.

Objectives

1. To decipher the record of Neogene environmental changes in the Maldives sediment archive.

Cores and downhole logs allowed us to produce a solid record and reconstruct Neogene environmental changes in the central Indian Ocean. Site U1468 cored the entire succession from the upper Oligocene to Pleistocene. Deeper cores recovered illustrate how an Oligocene neritic carbonate platform drowned and how sedimentation turned to a hemipelagic mode. Coinciding with the Oligocene to Miocene transition, the sedimentary regime changed to a pelagic system characterized by events with high organic accumulation. The record of the sea level-controlled lower and middle Miocene carbonate platform was cored at Sites U1466 and U1467. The onset of the monsoon wind-driven depositional system was cored at Sites U1466–U1468 and U1471. Preliminary shipboard analyses allow precise dating of this major paleoclimatological and paleoceanographical change, as it also applies to the extension of the Oxygen Minimum Zone into this part of the Indian Ocean. Coring produced a solid framework to foster postexpedition research of these distinct topics. We therefore regard this objective as fully accomplished.

2. To place the Maldives current system into the larger scale ocean current framework present during Neogene global cooling and monsoon evolution.

Seismic data from the Maldives document mounded drift packages deposited by the ocean currents that sweep through the Inner Sea. Today these currents are linked directly to the monsoon as they flow from west to east during the summer monsoon and reverse direction with the onset of the winter monsoon. This changing current also occurred during Expedition 359 and served as a good illustration of the sedimentary and oceanographic dynamics of the archipelago. Based on seismic stratigraphy, the onset of drift deposition coincides with cessation of sea level-controlled platform progradation during the late middle Miocene global cooling phase. If the Miocene drift deposits are related to the monsoon, as they are today, the onset of the drift deposits give strong evidence of the onset or at least major strengthening of the monsoon at this time. The biostratigraphic age model of Expedition 359 indicates a late middle Miocene age for the onset.

Complete spliced sections and logging at key sites during Expedition 359 provide the potential to assemble a cycle-based astrochronology for the Neogene section in the Maldives. This high-resolution chronology will allow (1) assignment of independent ages to key biostratigraphic events in the Maldives for comparison with those from other tropical regions, (2) assignment of more precise ages for the major sequence boundaries and unconformities, and (3) evaluation of higher resolution sedimentation rate variations.

The age of the onset of the drift deposition and thus the current system in this part of the Indian Ocean is essentially the same as the onset of the Santaren Drift in the Bahamas that is formed by the Florida Current. Initial comparison shows that not only the onset but also the changes in sedimentation rates within the two drift bodies are coeval. Likewise, the onset of the current across the Marion Plateau, northeast Australia, is only slightly younger based on data from ODP Leg 194. The synchronous evolution of the drifts indicates that the onset of the current in the Atlantic, Pacific, and Indian Oceans was basically simultaneous. Postexpedition research will have to establish the extent of the lead and lag in each ocean.

3. To obtain a continuous carbon isotopic record to calibrate a platform and platform margin record with the pelagic record.

This objective was achieved by coring the platform tops at three sites (U1465, U1469, and U1470) and the entire Neogene periplatform strata at several sites at varying distances from the platform (U1468, U1467, and U1471). Together, the cored intervals provide a complete record of the carbon isotopic record of the platform and platform margin sediments. Because sedimentation rates are high to very high in these settings, these cores provide an expanded record that will be suitable for high-resolution carbon isotope stratigraphy. In the distal portions of the prograding clinofolds, sedimentation rates were between 3.2 and 4.4 cm/ky, and in the drift deposits, they reached 17 cm/ky. The base of the Neogene was penetrated at Site U1468, where the earliest Miocene succession was a shallow-water carbonate lagoonal environment that developed into a somewhat deeper basin, the paleo-*Inner Sea* of the Maldives, with fine-grained carbonates that also contain numerous dark organic-rich intervals. Together with the sediments of the overlying distal bottomset from the Kardiva platform in the west, these sediments will provide a continuous carbon isotopic record to the late middle Miocene. The overlying late middle Miocene to recent drift deposits were cored at Sites U1466–U1468 and U1471. Each of these sites covered a different age interval with a high sedimentation rate. Thus, the entire Neogene is cored, and we therefore obtained an ideal data set for shore-based analysis of carbon isotopes on both the organic and inorganic fractions. This will allow the record of carbon isotope change to be extended back in time from the approximate 8 My record, which was already measured on sediments from ODP Site 716, to ~25 Ma at Site U1468. A complete comparison will be possible not only with ODP Site 1007, which penetrated the entire Miocene, but also in relation to other platform and pelagic records over the same time period. This comparison will allow assessment of the extent to which platform carbonates record changes in the global carbon cycle and determine whether changes in the carbon isotopic composition of organic and inorganic components covary and the implications this has on the deep-time record.

Additional discoveries

1. Organic-rich layers that indicate early Miocene oxygen minima.

At Site U1466, coring recovered an upper Oligocene to lower Miocene alternation of chalky white wackestone and black organic-rich layers in the lower Miocene. At Site U1468, the same facies was recovered above neritic carbonates with large benthic foraminifers. Here, the succession with nannofossil chalk and black organic-rich sediments is approximately 90 m thick. Based on their position within the stratigraphic succession and the estimated water depth of the *Inner Sea* at the time, the presumed oxygen minima conditions

necessary for their formation must have formed a relatively shallow basin.

2. The shallow nature of a carbonate contourite fan.

Although the drift package in the Kardiva Channel was identified based on the geometries seen on the seismic data, the cores revealed a facies evolution that has far-reaching implications for interpretations of neritic carbonates. Together with lithologies from the cores, this drift is best classified as a contourite fan. No such system has been previously reported for carbonates. The reason this discovery will have major implications for carbonate sedimentology is that the facies within this drift is very similar to what has hitherto been described as, for example, neritic shoals, prograding delta lobes, and so on. For example, Site U1468 cores from the apex of the drift mound contain large benthic foraminiferal floatstones that resemble benthic foraminiferal shoals. Likewise, the prograding lobes of this contourite fan are very reminiscent of what might be called a tidal delta front. The documentation of this carbonate contourite fan will thus trigger reinterpretation of deposits with these characteristics in the ancient.

3. Advection dominance of fluid flow.

Early diagenesis is thought to be controlled by diffusion of seawater into the underlying sediments. This diffusion-related diagenesis generally produces a characteristic depth profile of the major anions and cations. A general lack of variation as found during Expedition 359 may result both from high rates of advection in the high-permeability drift sediments and from different geochemical profiles and carbonate diagenesis being present during the sedimentary history. Many workers assume that the present measured pore water profile might have been similar throughout the history of a particular site and used gradients in various elements and isotopes to calculate rates of neomorphism and recrystallization (Baker et al., 1982; Richter and DePaolo, 1987). Therefore, the findings made during Expedition 359 question one of the basic assumptions inherent in such modeling studies.

4. Planktonic foraminiferal and nannofossil biostratigraphy.

During Expedition 359, age models were constructed with a succession of well-constrained events of calcareous nannofossils and planktonic foraminifers, which generally were in good agreement. However, through much of the Pleistocene and Pliocene intervals in all cores there was a consistent offset between the ages inferred from calcareous nannofossil events and those from planktonic foraminifers, with the planktonic foraminifers suggesting ages about 0.5 My older than the calcareous nannofossils. This persistent pattern indicates that possibly the age calibrations of these events need revision, at least for the Maldives (i.e., the central Indian Ocean).

References

- Anselmetti, F.S., Eberli, G.P., and Ding, Z.-D., 2000. From the Great Bahama Bank into the Straits of Florida: a margin architecture controlled by sea-level fluctuations and ocean currents. *Geological Society of America Bulletin*, 112(6):829–844. [http://dx.doi.org/10.1130/0016-7606\(2000\)112<0829:FTGBBI>2.3.CO;2](http://dx.doi.org/10.1130/0016-7606(2000)112<0829:FTGBBI>2.3.CO;2)
- Arthur, M.A., and Schlanger, S.O., 1979. Cretaceous “oceanic anoxic events” as causal factors in development of reef-reservoired giant oil fields. *AAPG Bulletin*, 63:870–885.
- Aubert, O., and Droxler, A.W., 1992. General Cenozoic evolution of the Maldives carbonate system (equatorial Indian Ocean). *Bulletin Des Centres de Recherches Exploration-Production Elf-Aquitaine*, 16(1):113–136.
- Aubert, O., and Droxler, A.W., 1996. Seismic stratigraphy and depositional signatures of the Maldives carbonate system (Indian Ocean). *Marine and Petroleum Geology*, 13(5):503–536. [http://dx.doi.org/10.1016/0264-8172\(96\)00008-6](http://dx.doi.org/10.1016/0264-8172(96)00008-6)
- Backman, J., Duncan, R.A., et al., 1988. *Proceedings of the Ocean Drilling Program, Initial Reports*, 115: College Station, TX (Ocean Drilling Program). <http://dx.doi.org/10.2973/odp.proc.ir.115.1988>
- Baker, P.A., Gieskes, J.M., and Elderfield, H., 1982. Diagenesis of carbonates in deep-sea sediments: evidence from Sr/Ca ratios and interstitial dissolved Sr²⁺ data. *Journal of Sedimentary Research*, 52(1):71–82. <http://dx.doi.org/10.1306/212F7EE1-2B24-11D7-8648000102C1865D>
- Belopolsky, A.V., and Droxler, A.W., 2004a. Seismic expressions and interpretation of carbonate sequences: the Maldives platform, equatorial Indian Ocean. *AAPG Studies in Geology*, 49. <http://archives.datapages.com/data/specpubs/study49/images/st49.pdf>
- Belopolsky, A.V., and Droxler, A.W., 2004b. Seismic expressions of prograding carbonate bank margins: middle Miocene, Maldives, Indian Ocean. In Eberli, G.P., Masafiero, J.L., and Sarg, J.F. (Eds.), *Seismic Imaging of Carbonate Reservoirs and Systems*. AAPG Memoir, 81:267–290. <http://archives.datapages.com/data/specpubs/memoir81/CHAPTER12/CHAPTER12.CHAPTER12.HTM>
- Betzler, C., Eberli, G.P., Alvarez Zarikian, C.A., Alonso-García, M., Bialik, O.M., Blättler, C.L., Guo, J.A., Haffen, S., Horozal, S., Inoue, M., Jovane, L., Kroon, D., Lanci, L., Laya, J.C., Ling Hui Mee, A., Lüdmann, T., Nakakuni, M., Nath, B.N., Niino, K., Petruny, L.M., Pratiwi, S.D., Reijmer, J.J.G., Reolid, J., Slagle, A.L., Sloss, C.R., Su, X., Swart, P.K., Wright, J.D., Yao, Z., and Young, J.R., 2017. Site U1471. In Betzler, C., Eberli, G.P., Alvarez Zarikian, C.A., and the Expedition 359 Scientists, *Maldives Monsoon and Sea Level*. Proceedings of the International Ocean Discovery Program, 359: College Station, TX (International Ocean Discovery Program). <http://dx.doi.org/10.14379/iodp.proc.359.109.2017>
- Betzler, C., Fürstenau, J., Lüdmann, T., Hübscher, C., Lindhorst, S., Paul, A., Reijmer, J.J.G., and Droxler, A.W., 2013a. Sea-level and ocean-current control on carbonate-platform growth, Maldives, Indian Ocean. *Basin Research*, 25(2):172–196. <http://dx.doi.org/10.1111/j.1365-2117.2012.00554.x>
- Betzler, C., Hübscher, C., Lindhorst, S., Reijmer, J.J.G., Römer, M., Droxler, A.W., Fürstenau, J., and Lüdmann, T., 2009. Monsoon-induced partial carbonate platform drowning (Maldives, Indian Ocean). *Geology*, 37(10):867–870. <http://dx.doi.org/10.1130/G25702A.1>
- Betzler, C., Kroon, D., and Reijmer, J.J.G., 2000. Synchronicity of major late Neogene sea level fluctuations and paleoceanographically controlled changes as recorded by two carbonate platforms. *Paleoceanography*, 15(6):722–730. <http://dx.doi.org/10.1029/1999PA000481>
- Betzler, C., Lindhorst, S., Lüdmann, T., Weiss, B., Wunsch, M., and Braga, J.C., 2015. The leaking bucket of a Maldives atoll: implications for the understanding of carbonate platform drowning. *Marine Geology*, 366:16–33. <http://dx.doi.org/10.1016/j.margeo.2015.04.009>
- Betzler, C., Lüdmann, T., Hübscher, C., and Fürstenau, J., 2013b. Current and sea-level signals in periplatform ooze (Neogene, Maldives, Indian Ocean). *Sedimentary Geology*, 290:126–137. <http://dx.doi.org/10.1016/j.sedgeo.2013.03.011>
- Ciarapica, G., and Passeri, L., 1993. An overview of the Maldivian coral reefs in Felidu and North Malé atoll (Indian Ocean): platform drowning by ecological crises. *Facies*, 28(1):33–65. <http://dx.doi.org/10.1007/BF02539727>
- Clift, P.D., Hodges, K.V., Heslop, D., Hannigan, R., Long, H.V., and Calves, G., 2008. Correlation of Himalayan exhumation rates and Asian monsoon intensity. *Nature Geoscience*, 1(12):875–880. <http://dx.doi.org/10.1038/ngeo351>
- Dickens, G.R., and Owen, R.M., 1994. Late Miocene–early Pliocene manganese redirection in the central Indian Ocean: expansion of the intermediate water oxygen minimum zone. *Paleoceanography*, 9(1):169–181. <http://dx.doi.org/10.1029/93PA02699>
- Droxler, A.W., Haddad, G.A., Mucciarone, D.A., and Cullen, J.L., 1990. Pliocene–Pleistocene aragonite cyclic variations in Holes 714A and 716B

- (The Maldives) compared with Hole 633A (The Bahamas): records of climate-induced CaCO₃ preservation at intermediate water depths. *In* Duncan, R.A., Backman, J., Peterson, L.C., et al., *Proceedings of the Ocean Drilling Program, Scientific Results*, 115: College Station, TX (Ocean Drilling Program), 539–577. <http://dx.doi.org/10.2973/odp.proc.sr.115.179.1990>
- Duncan, R.A., and Hargraves, R.B., 1990. ⁴⁰Ar/³⁹Ar geochronology of basement rocks from the Mascarene Plateau, the Chagos Bank, and the Maldives Ridge. *In* Duncan, R.A., Backman, J., Peterson, L.C., et al., *Proceedings of the Ocean Drilling Program, Scientific Results*, 115: College Station, TX (Ocean Drilling Program), 43–51. <http://dx.doi.org/10.2973/odp.proc.sr.115.141.1990>
- Eberli, G.P., 1991. Growth and demise of isolated carbonate platforms: Bahamian controversies. *In* Müller, D., McKenzie, J., and Weissert, H. (Eds.), *Controversies in Modern Geology: Evolution of Geological Theories in Sedimentology, Earth History and Tectonics*: London (Academic Press), 231–248.
- Eberli, G.P., Anselmetti, F.S., Isern, A.R., and Delius, H., 2010. Timing of changes in sea-level and currents along Miocene platforms on the Marion Plateau, Australia. *In* Morgan, W.A., George, A.D., Harris, P.M., Kupecz, J.A., and Sarg, J.F. (Eds.), *Cenozoic Carbonate Systems of Australasia*. Special Publication - SEPM (Society for Sedimentary Geology), 95:219–242. <http://dx.doi.org/10.2110/sepm.sp.095.219>
- Eberli, G.P., Anselmetti, F.S., Kroon, D., Sato, T., and Wright, J.D., 2002. The chronostratigraphic significance of seismic reflections along the Bahamas Transect. *Marine Geology*, 185(1–2):1–17. [http://dx.doi.org/10.1016/S0025-3227\(01\)00287-0](http://dx.doi.org/10.1016/S0025-3227(01)00287-0)
- Fürstenau, J., Lindhorst, S., Betzler, C., and Hübscher, C., 2010. Submerged reef terraces of the Maldives (Indian Ocean). *Geo-Marine Letters*, 30(5):511–515. <http://dx.doi.org/10.1007/s00367-009-0174-2>
- Gischler, E., 2006. Sedimentation on Rasdhoo and Ari atolls, Maldives, Indian Ocean. *Facies*, 52(3):341–360. <http://dx.doi.org/10.1007/s10347-005-0031-3>
- Gischler, E., Hudson, J.H., and Pisera, A., 2008. Late Quaternary reef growth and sea level in the Maldives (Indian Ocean). *Marine Geology*, 250(1–2):104–113. <http://dx.doi.org/10.1016/j.margeo.2008.01.004>
- Gupta, A.K., Yuvarja, A., Prakasam, M., Clemens, S.C., and Velu, A., 2015. Evolution of the South Asian monsoon wind system since the late middle Miocene. *Palaeogeography, Palaeoclimatology, Palaeoecology*, 438:160–167. <http://dx.doi.org/10.1016/j.palaeo.2015.08.006>
- Hallock, P., and Schlager, W., 1986. Nutrient excess and the demise of coral reefs and carbonate platforms. *Palaios*, 1(4):389–398. <http://dx.doi.org/10.2307/3514476>
- Isern, A.R., Anselmetti, F.S., and Blum, P., 2004. A Neogene carbonate platform, slope, and shelf edifice shaped by sea level and ocean currents, Marion Plateau (northeast Australia). *In* Eberli, G.P., Masferro, J.L., and Sarg, J.F. (Eds.), *Seismic Imaging of Carbonate Reservoirs and Systems*. AAPG Memoir, 81:291–307. <http://archives.datapages.com/data/spec-pubs/memoir81/CHAPTER13/CHAPTER13.HTM>
- John, C.M., and Mutti, M., 2005. Relative control of paleoceanography, climate, and eustasy over heterozoan carbonates: a perspective from slope sediments of the Marion Plateau (ODP Leg 194). *Journal of Sedimentary Research*, 75(2):216–230. <http://dx.doi.org/10.2110/jsr.2005.017>
- Kroon, D., Steens, T., and Troelstra, S.R., 1991. Onset of monsoonal related upwelling in the western Arabian Sea as revealed by planktonic foraminifers. *In* Prell, W.L., Niitsuma, N., et al., *Proceedings of the Ocean Drilling Program, Scientific Results*, 117: College Station, TX (Ocean Drilling Program), 257–263. <http://dx.doi.org/10.2973/odp.proc.sr.117.126.1991>
- Lüdmann, T., Kalvelage, C., Betzler, C., Fürstenau, J., and Hübscher, C., 2013. The Maldives, a giant isolated carbonate platform dominated by bottom currents. *Marine and Petroleum Geology*, 43:326–340. <http://dx.doi.org/10.1016/j.marpetgeo.2013.01.004>
- Malone, M.J., Baker, P.A., Burns, S.J., and Swart, P.K., 1990. Geochemistry of periplatform carbonate sediments, Leg 115, Site 716 (Maldives archipelago, Indian Ocean). *In* Duncan, R.A., Backman, J., Peterson, L.C., et al., *Proceedings of the Ocean Drilling Program, Scientific Results*, 115: College Station, TX (Ocean Drilling Program), 647–659. <http://dx.doi.org/10.2973/odp.proc.sr.115.184.1990>
- Malone, M.J., Slowey, N.C., and Henderson, G.M., 2001. Early diagenesis of shallow-water periplatform carbonate sediments, leeward margin, Great Bahama Bank (Ocean Drilling Program Leg 166). *Geological Society of America Bulletin*, 113(7):881–894. [http://dx.doi.org/10.1130/0016-7606\(2001\)113<0881:EDOSWP>2.0.CO;2](http://dx.doi.org/10.1130/0016-7606(2001)113<0881:EDOSWP>2.0.CO;2)
- Paul, A., Reijmer, J.J.G., Fürstenau, J., Kinkel, H., and Betzler, C., 2012. Relationship between late Pleistocene sea-level variations, carbonate platform morphology and aragonite production (Maldives, Indian Ocean). *Sedimentology*, 59(5):1540–1658. <http://dx.doi.org/10.1111/j.1365-3091.2011.01319.x>
- Philip, J., and Schlager, W., 1990. Cretaceous carbonate platforms. *In* Ginsburg, R.N., and Beaudoin, B. (Eds.), *Nato Science Series C (Volume 304): Cretaceous Resources, Events and Rhythms: Background and Plans for Research*: Dordrecht, The Netherlands (Springer), 173.
- Prell, W.L., Murray, D.W., Clemens, S.C., and Anderson, D.M., 1992. Evolution and variability of the Indian Ocean summer monsoon: evidence from the western Arabian Sea drilling program. *In* Duncan, R.A., Rea, D.K., Kidd, R.B., von Rad, U., and Weissel, J.K. (Eds.), *Synthesis of Results from Scientific Drilling in the Indian Ocean*. Geophysical Monograph, 70:447–469. <http://dx.doi.org/10.1029/GM070p0447>
- Preu, C., and Engelbrecht, C., 1991. Patterns and processes shaping the present morphodynamics of coral reef islands—case study from the North-Male atoll, Maldives (Indian Ocean). *In* Brückner, H., and Radtke, U. (Eds.), *From the North Sea to the Indian Ocean*: Stuttgart, Germany (Franz Steiner), 209–220.
- Purdy, E.G., and Bertram, G.T., 1993. *Carbonate Concepts from the Maldives, Indian Ocean*. AAPG Studies in Geology, 34. <http://archives.datapages.com/data/specpubs/carbo-nal/data/a047/a047/0001/0000/0007.htm>
- Rea, D.K., 1992. Delivery of Himalayan sediment to the northern Indian Ocean and its relation to global climate, sea level, uplift, and seawater strontium. *In* Duncan, R.A., Rea, D.K., Kidd, R.B., von Rad, U., and Weissel, J.K. (Eds.), *Synthesis of Results from Scientific Drilling in the Indian Ocean*. Geophysical Monograph, 70:387–402. <http://dx.doi.org/10.1029/GM070p0387>
- Richter, F.M., and DePaolo, D.J., 1987. Numerical models for diagenesis and the Neogene Sr isotopic evolution of seawater from DSDP Site 590B. *Earth and Planetary Science Letters*, 83(1–4):27–38. [http://dx.doi.org/10.1016/0012-821X\(87\)90048-3](http://dx.doi.org/10.1016/0012-821X(87)90048-3)
- Schlager, W., 1981. The paradox of drowned reefs and carbonate platforms. *Geological Society of America Bulletin*, 92(4):197–211. [http://dx.doi.org/10.1130/0016-7606\(1981\)92<197:TPO-DRA>2.0.CO;2](http://dx.doi.org/10.1130/0016-7606(1981)92<197:TPO-DRA>2.0.CO;2)
- Swart, P.K., 2008. Global synchronous changes in the carbon isotopic composition of carbonate sediments unrelated to changes in the global carbon cycle. *Proceedings of the National Academy of Sciences of the United States of America*, 105(37):13741–13745. <http://dx.doi.org/10.1073/pnas.0802841105>
- Tomczak, M., and Godfrey, J.S., 2003. *Regional Oceanography: An Introduction* (2nd ed.): Delhi (Daya Publishing House).
- Zampetti, V., Schlager, W., van Konijnenburg, J.-H., and Everts, A.-J., 2004. Architecture and growth history of a Miocene carbonate platform from 3D seismic reflection data: Luconia province, offshore Sarawak, Malaysia. *Marine and Petroleum Geology*, 21(5): 517–534. <http://dx.doi.org/10.1016/j.marpetgeo.2004.01.006>
- Zheng, H., Powell, C.M., Rea, D.K., Wang, J., and Wang, P., 2004. Late Miocene and mid-Pliocene enhancement of the East Asian monsoon as viewed from the land and sea. *Global and Planetary Change*, 41(3–4):147–155. <http://dx.doi.org/10.1016/j.gloplacha.2004.01.003>